COLLOID DETACHMENT FROM ROUGH SURFACES IN THE ENVIRONMENT

by

Ryan P. Neyland

A Thesis

Submitted to the Faculty

of

WORCESTER POLYTECHNIC INSTITUTE

In Partial fulfillment of the requirements for the

Degree of Master of Science

In

Environmental Engineering

By

_____

May 2005

APPROVED:

_____

Professor John Bergendahl, Major Advisor

_____

Professor Terri Camesano, Co-Advisor

_____

Professor Frederick Hart, Head of Department

ACKNOWLEDGEMENTS

Mr. Ryan Neyland was funded by a teaching assistantship provided by the Civil and Environmental Engineering Department at WPI. The research was completed in full at WPI. The majority of the work was done using the resources in the water quality laboratory. The roughness was measured using the AFM in the Chemical Engineering Department.

This research was completed with the help and assistance of many people. I want to thank the Civil and Environmental Engineering Department at WPI for supporting me through two years including summers through teaching assistantships. Next, I would like to thank Dr. John Bergendahl for his guidance, support, and expertise. This research could not have been completed without his time and assistance. I want to thank Dr. Terri Camesano for her support and assistance and for providing me with access to the AFM in the Chemical Engineering Department. I would like to thank Ray Emerson for his expertise in operating the AFM and the time he spent assisting with roughness measurements. I want to thank Don Pellegrino for maintaining the high quality of the laboratory. I would also like to thank Shawn Hallinan for his knowledge with statistical testing. Finally, I want to thank my family for their continuous motivation and words of encouragement. I want to specifically thank my brother Erik for his continuous advice throughout my time at WPI.

TABLE OF CONTENTS

LIST OF TABLES

LIST OF ILLUSTRATIONS

ABSTRACT

Colloid detachment and mobilization can be of significant interest to those studying colloid behavior in the environment. The transport of pathogens such as viruses, bacteria, and protozoa can cause health problems in animals and humans. The transport of organics, radionuclides, and other hydrophobic contaminants can be enhanced by adsorption to mobilized colloid surfaces. Research has been done by others quantifying the detachment of colloids from smooth porous media. Real surfaces in the environment and engineered systems are rough.

Glass beads were chemically roughened by procedures similar to those from Shellenberger and Logan (2002) and Itälä et al. (2001) using chromic acid and a citric acid/ammonium fluoride solution. Surface asperities were measured using Atomic Force Microscopy (AFM), and the roughness was defined by three parameters: Root Mean Square (RMS) roughness, peak to valley height (P/V height), and peak to peak distance (λ). Detachment from the chemically etched porous media was measured in column tests. The controlling roughness parameter between the two batches of beads was found to be λ.

A theoretical model to predict the effect of roughness on detachment was developed. Using a moment balance around the downstream point of contact, the parameters incorporated into the model were particle diameter, P/V height, and λ. The model predicted the shear required for colloid detachment in column tests. Surface roughness was found to significantly inhibit colloid detachment.

INTRODUCTION AND BACKGROUND

Colloid attachment and detachment from porous media surfaces has been the subject of investigation for numerous environmental reasons. Porous media is used in many engineering operations and is found in many natural systems as well. Some related environmental issues involve colloid and contaminant transport in groundwater, colloid attachment and detachment within engineered sand filters, and pollutant removal from contaminated sites. Any situation involving fluid flow such as air or water through porous media will be concerned with colloid detachment and transport. The desire for colloid attachment or detachment is system dependent, and there are many cases in which both are required at alternate times. Due to the range of implications involving either attachment or detachment from porous media surfaces, the conditions and mechanisms under which both occur are vital for understanding these engineered and natural systems. Much of the initial attention by researchers was given to determining the mechanisms and reasons for colloid attachment. Recently, the mechanisms for detachment have become the center point for investigation and research.

For particles attached to the surface of porous media to become detached, a disturbance to the system must occur. This perturbation may involve a change in the solution chemistry or an alteration of the hydrodynamics of the system. Amirtharajah and Raveendran (1993) studied the detachment of latex particles with diameters of 2.0 μm and 5.0 μm from glass beads. Their experiments concluded that particle detachment was dependent on the ionic strength of the detachment solution. Higher detachment efficiencies were found for solutions having lower ionic strength. Freitas and Sharma (1999) showed the effects of the electrostatic double layer on the detachment of

polystyrene particles from a silica substrate. When using deionized water in a flow cell, a repulsive electrostatic double layer existed and experiments illustrated that significant detachment was possible. When using a 0.1 M solution of potassium chloride, the repulsive electrostatic double layer is minimal and nearly all of the polystyrene particles remained attached.

Bai and Tien (1997) focused their study on particle detachment in deep bed filtration. The purpose of the study was to analyze several factors which may have an effect on particle detachment and to perform experimental research to support their conclusions. Bai and Tien found that larger particles were more likely to detach from media surfaces. Particles identical in size had a greater tendency for detachment from larger grain (media) sizes, and detachment became more significant at higher headloss gradients.

Ryan and Elimelech (1996) provided an extensive review on colloid mobilization and transport in groundwater systems. The review identified field tests that showed colloid mobilization due to decreasing ionic strength and increasing pH. The review also suggested that increasing the groundwater flow contributes to colloid detachment and transport in the environment. Ryan and Gschwend (1994) investigated the effects of ionic strength and flowrate on the detachment of hematite colloids from quartz surfaces in a packed bed. Experimental results showed an increase in colloid mobilization with decreasing ionic strength and increasing flowrate.

Bergendahl and Grasso (1999) used an extended-DLVO model to successfully predict the pH necessary to detach colloids from media surfaces using ionic strengths ranging from 0.01 M NaCl to approximately zero (deionized water). The DLVO theory

developed by Derjaguin and Landau (1941) and Verwey and Overbeek (1948) incorporates only the van der Waals attraction and the electrical double layer repulsion when modeling colloidal interactions. The extended-DLVO model incorporates Born repulsion (Ruckenstein and Prieve, 1976) and Lewis acid-base (van Oss, 1994) interaction energies. In a subsequent study, Bergendahl and Grasso (2000) determined that a hydrodynamic shear of 100.6 s^{-1} in a packed bed removed 50% of the particles which were not removed by altering the solution chemistry alone. The primary mechanism for hydrodynamic detachment was considered to be rolling. Using the hysteresis loss factor for rolling for polystryrene and a gamma distribution of the residual particle fraction interaction energy, the detachment due to changes in flowrate in the packed bed was well predicted. Bergendahl and Grasso (1998) also showed particle detachment during toxicity characteristic leaching procedure (TCLP) testing of a coal-tar contaminated soil. The rolling mechanism was hypothesized to be the cause for colloid detachment. The mechanical agitation occurring in the batch test provided the shear for rolling and therefore detachment.

A great deal of research on colloid detachment from porous glass beads in packed columns has been done by several investigators (Kallay et al., 1987; Tobiason, 1989; Elimelech, 1994; Liu et al, 1995; Rijnaarts et al, 1996; Bergendahl and Grasso, 1998, 1999, 2000). In general, the primary objectives of most studies were to investigate the effects of solution chemistry and hydrodynamic shear on the detachment mechanism. These studies often use identical batches of smooth, spherical glass beads which are cleaned prior to being used as media in packed column tests. The interactions and attachments between the colloids and media surfaces are often modeled as a sphere

attached to a smooth, flat plate at one point. However, in the environment, porous media surfaces are not smooth and may have significant surface asperities.

The roughness of porous media surfaces such as glass beads has been successfully measured and altered. Shellenberger and Logan (2002) used a method previously developed by Litton and Olsen (1993) to chemically roughen glass beads. The glass beads were sequentially soaked and rinsed with deionized water in the following solutions: 36.5-38% HCl, 10% H_2CrO_4, 36.5-38% HCl, and dried. The glass beads were made smoother by soaking them in 12.5 M NaOH for 30 minutes followed by rinsing them in ultrapure water. The root-mean-square roughness (RMS) of the beads treated with chromic acid was 38.1 ± 3.9 nm, while the RMS of the beads treated with sodium hydroxide was significantly less at 15.0 ± 1.9 nm. Shellenberger and Logan found that there was a greater retention of latex microspheres on the rougher glass beads which were chemically etched using the chromic acid procedure. The collision efficiencies for the rough glass beads were 30-50% larger than for the smooth beads. Bacteria displayed an overall trend of greater retention on rough rather than smooth surfaces. However, the results were not as significant as with the latex microspheres due to low values for collision efficiencies and variability in results from identical column tests.

Itälä et al. (2001) looked at enhancing the bioactivity of glass surfaces by increasing the surface roughness. The roughness increased the potential surface area for both cell attachment and interaction between the cells and the bio-material. Two of the etching procedures used involved soaking the glass in a HF (14.6 M)/H_2O solution for 30-480 seconds and in a NH_4F (22 M)/$C_8H_{10}O_7$ (8.5 M) for 60-1800 seconds. The RMS of the glass chemically etched using the ammonium fluoride and citric acid ranged from

420-640 nm. In the study, it was shown that chemical etching of the glass surface did not interfere with the characteristic surface reactions of bioactive glasses.

Rabinovich et al. (2000) developed two types of roughness profiles in their investigation on the adhesion between nanoscale rough surfaces. Rabinovich et al. defined a primary roughness involving an RMS_1 associated with a peak to peak distance, λ_1, of approximately 1000 nm and a secondary roughness which involved an RMS_2 associated with a λ_2 value of approximately 250 nm. Beach et al. (2001) developed a roughness analysis based on the Rabinovich et al. approach. RMS_1 and λ_1 values were determined from Atomic Force Microscope (AFM) images which were 20 x 20 μm in size. The secondary roughness RMS_2 and λ_2 values were determined by dividing the 20 x 20 μm image into 16 images which were 5 x 5 μm in size. Four of these 16 smaller images were analyzed in the same manner as done for the whole 20 x 20 μm image to find the secondary roughness parameters.

Ryde and Matijević (2000) investigated the detachment of spherical chromium hydroxide particles from steel beads in column tests. After an initial deposition phase, the metal oxide particles were detached by rinsing the packed bed with solutions of varying pH and ionic strength. Ryde and Matijević found increasing detachment with decreases in ionic strength and increases in pH. The study and discussion dealing with these specific metal oxide particles is particularly interesting. In all of the other column tests using smooth media such as cleaned glass beads in which Ryde and Matijević measured detachment, complete removal was demonstrated. However, in the detachment tests using the chromium hydroxide particles deposited on steel beads, it was impossible to achieve complete removal. According to Ryde and Matijević, the reason for this

unique behavior was the roughness of the media surface. The particles were hypothesized to have been trapped in the crevices of the metal surface and could not be removed.

Previous colloid detachment studies have been performed with porous media that was assumed to be smooth. The objective of this research was to investigate the effects of media surface roughness on the detachment of colloids from packed beds of granular media. The fundamental models and relationships developed in previous studies were used along with measured roughness parameters to develop a new theoretical model. The model was used to predict the hydrodynamic shear required to remove attached colloids from porous media. Experimental detachment results from packed bed column tests were used to show the validity of the theoretical model.

Hypotheses:

- **Colloid detachment is affected by roughness**
- **Colloid detachment from rough surfaces with hydrodynamic shear changes can be predicted**

MATERIALS AND METHODS

Glassware

All glassware was sequentially washed in water with Sparkleen laboratory detergent (Fisher Scientific, Pittsburgh, PA; soaked approximately 24h), nitric acid (20 %, diluted from 70 % HNO_3, Fisher Scientific, Pittsburgh, PA; soaked approximately 24 h), and deionized water (ROpure ST, Barnstead/Thermolyne, Dubuque, IA; soaked approximately 24 h). All glassware was allowed to air dry overnight and was stored in a laboratory cabinet which held only equipment used for this research.

Cleaning and Roughening of Glass Beads

The glass column was packed with glass beads (Sigma Chemical Company, St. Louis, MO) which were 425 to 600 μm in diameter. The glass beads were chemically cleaned in a 250 mL glass beaker before use by rinsing sequentially with acetone, hexane (99.6 % and 99.9 % respectively, both Fisher Scientific, Pittsburgh, PA; soaked approximately 1 h), concentrated hydrochloric acid (37.3 % HCl, Fisher Scientific, Pittsburgh, PA; soaked approximately 12 h), and finally 0.1 M sodium hydroxide (made from 97 % NaOH pellets, Mallinckrodt Chemical Works, St. Louis, MO, New York, NY; 3 soakings of approximately 5 min each). Repeated rinsings with deionized water were made in between each sequential rinse during the cleaning process in order to remove all of the previous rinsing solution before adding the next (approximately 4 repeated 5 min rinsings). The glass beads were dried overnight at 110ºC after the hexane rinse and again after the NaOH rinses and were then transferred to a sealed 250 mL Nalgene bottle and stored until further use.

Two methods were used to chemically roughen the smooth, cleaned glass beads. In the first method following a procedure modified from Shellenberger and Logan, the glass beads were chemically roughened in a 250 mL Nalgene bottle by rinsing sequentially in concentrated HCl, chromic acid (10 % H_2CrO_4, Fisher Scientific, Pittsburgh, PA), and then again in concentrated HCl. There were three different sets of roughened glass beads based on the amount of time each rinse was used. The three sets included beads that were rinsed using 6, 12, 24 h intervals. For example, using the 6 h intervals, the beads were rinsed for 6 h in concentrated HCl, then for 6 h in the H_2CrO_4 solution, and then once again in concentrated HCl for 6 h. Repeated rinsings with deionized water were made in between each rinse in order to remove the previous solution from the bottle before the next rinse was added (approximately 4 repeated 5 min rinsings). The glass beads were transferred to a 100 mL glass beaker and dried at 110ºC after the final rinse. The beads were finally transferred to a 250 mL Nalgene bottle and stored until the roughness of the glass beads was tested as described below.

The second approach following a procedure modified from Itälä et al. was used to roughen the glass beads used a solution of 7.7M ammonium fluoride (NH_4F)/3.0M citric acid ($C_6H_8O_7$). Eighty grams of smooth, cleaned glass beads were placed in a 250 mL HDPE Nalgene bottle. In a second 250 mL Nalgene bottle which was used to make the rinsing solution, 70 mL of deionized water was added. Using hexagonal polystyrene weighing dishes, 20 grams of crystal NH_4F (98.1% NH_4F, Fisher Scientific, Pittsburgh, PA) and 40 grams of anhydrous $C_6H_8O_7$ (100.5% $C_6H_8O_7$, Fisher Scientific, Pittsburgh, PA) was added to the Nalgene bottle. The 7.7M NH_4F/3.0M $C_6H_8O_7$ was added to the first Nalgene bottle where the glass beads soaked in solution for 30 minutes. After the 30

minute rinse was complete, the roughened glass beads were rinsed with deionized water to remove the 7.7M NH_4F/3.0M $C_6H_8O_7$. Ethanol (95% denatured ethyl alcohol, Fisher Scientific, Pittsburgh, PA) was then used to rinse the glass beads followed by deionized water to remove the ethanol. A final rinse with 1M hydrochloric acid (made from diluting 37.3% HCl, Fisher Scientific, Pittsburgh, PA) to remove any residue of precipitated salts from the glass beads was used. The 1M HCl was removed by repeated rinsings with deionized water. The final product of roughened glass beads was placed in a 100 mL glass beaker and dried overnight at 105°C. After drying, the roughened glass beads were transferred to a clean 250 mL HDPE Nalgene bottle where they were covered and stored until further use.

Analysis of Surface Roughness

The analysis of the surface roughness for each batch of chemically roughened glass beads was conducted with atomic force microscopy (AFM, Digital Instruments/Veeco Metrology Group, Santa Barbara, CA, USA). The AFM was a Dimension 3100 AFM with a Nanoscope IIIa controller. The two batches of glass beads were analyzed using the AFM. The first batch consisted of glass beads that were chemically etched by soaking them in chromic acid for 12 hours, and the second batch consisted of glass beads which were soaked and roughened in a citric acid/ammonium fluoride solution.

A thin layer of epoxy was spread on a microscope slide and allowed to slightly dry and harden for approximately 30 seconds. A layer of glass beads was sprinkled on the epoxy and dried completely before being stored in a desiccator. The epoxy was allowed to dry for 30 seconds before the layer of glass beads were sprinkled on top so

that the beads would stick to the epoxy when dried but would also be elevated above the layer of epoxy. This was necessary in order for the AFM probe to tap the surface of the beads and not tap the actual epoxy layer. The epoxy would cause the probe to stick to the surface and would in turn give an incorrect measurement of surface height.

The AFM was used to tap and measure the surface height on three different beads for each batch. On each of these three beads, the AFM measured three surface areas of 25.0 μm^2 with dimensions of 5.0 μm x 5.0 μm. Thus, for each batch of beads, a total of nine surface areas were measured in order to provide some statistical information when analyzing the data. Within the 25.0 μm^2 area, the AFM measured the surface height of the bead by tapping the surface in a matrix of 512 x 512 points. This analysis resulted in a data spreadsheet which contained 512 rows by 512 columns with the surface height measurement in nanometers (nm) given for each point within the matrix. The surface height was designated as the z-direction and the rows and columns represented movement in the x-direction and y-direction respectively. Therefore, with the total distance in either the x-direction or y-direction being 5000 nm and the matrix containing 512 rows and 512 columns, the distance from one point in the matrix to the next when moving in either the x-direction or y-direction was approximately 9.76 nm.

With the data for each of the 27 bead areas (three 25.0 μm^2 surface areas on three different beads for each of three batches) collected and transferred into a spreadsheet in SigmaPlot (Sigmaplot 8.0.2, Systat Inc., 2002), the roughness for each of the three batches of beads could be analyzed using different roughness metrics. The first parameter used to analyze the surface was the root mean square (RMS) roughness. RMS can be determined using Equation 1.

$$\mathrm{RMS} = \sqrt{\frac{\sum (Z_i - Z_{ave})^2}{N}} \tag{1}$$

In the analysis, an RMS_1 and an RMS_2 parameter were defined. The RMS_1 parameter was used to define the RMS value for the entire 25.0 μm^2 surface area while three RMS_2 values were used to define three smaller 0.25 μm^2 surface areas within the entire 25.0 μm^2 surface area. Using SigmaPlot, an RMS_1 value was determined for each bead area which meant that a total of nine RMS_1 values were estimated for each batch of beads. The mean of these nine values was used as the RMS_1 roughness for the selected batch of glass beads. Similarly, SigmaPlot was used to determine three RMS_2 values for each bead area which meant that a total of 27 RMS_2 values were estimated for each batch of beads. The mean of these 27 values was used as the RMS_2 roughness for the selected batch of glass beads. In regards to the RMS_2 roughness parameter, the same three 0.25 μm^2 surface areas were used for each measurement. The three surface areas were defined by same three matrices in SigmaPlot each time. In SigmaPlot, a matrix is defined by ($column_{start}$, row_{start}, $column_{end}$, row_{end}). The three matrices used for each bead area to determine the three RMS_2 values were (10,10,61,61), (176,176,227,227), and (375,375,426,426). An overall RMS value was calculated using Equation 2.

$$\mathrm{RMS}_{\mathrm{OVERALL}} = \sqrt{\mathrm{RMS}_1^{\,2} + \mathrm{RMS}_2^{\,2}} \tag{2}$$

The second parameter used to define surface roughness was the peak to peak distance (λ), the distance between peaks on the surfaces. Similar to the RMS roughness parameter, a primary peak to peak distance (λ_1) and a secondary peak to peak value (λ_2) were defined. Three primary peak to peak values were determined for each bead area. Using SigmaPlot, the cross sections of columns 35, 201, and 400 were illustrated. The

total distance displayed on each cross section was 5000 nm. Using the total cross section, a λ_1 value was estimated for each of the columns. With three λ_1 values for each bead area, a total of 27 λ_1 values were recorded for each batch of glass beads. The mean of these 27 values defined the λ_1 parameter. The λ_2 parameter was determined using a similar process. The same cross sections of columns 35, 201, and 400 were used. Three 500 nm sub-sections within each column cross section were then magnified using SigmaPlot. The three sub-sections used were 1000 – 1500 nm, 2000 – 2500 nm, and 3500 – 4000 nm. Within each of these sub-sections, the peak to peak distance was measured and represented a value for λ_2. With a total of nine λ_2 values estimated for each bead area, a total of 81 λ_2 values were recorded for each batch of beads. The mean of these 81 values defined the λ_2 parameter.

The third and final parameter used to define surface roughness was the peak to valley height. The peak to valley height (P/V height) is defined as the distance from the top of peak to the bottom of the adjacent valley. Using the total cross sections of columns 35, 201, and 400 in SigmaPlot, the maximum P/V height was located and measured within each 5000 nm cross section. A total of three P/V heights were determined for each bead area meaning that 27 P/V heights were measured for each batch of glass beads. The mean of these 27 values was used to represent the P/V height parameter.

Colloids

Surfactant-free carboxyl white polystyrene latex microspheres of different sizes (Interfacial Dynamics Corporation, Portland, OR) were used. There were three sets of microspheres ranging in size from 0.12 μm to 1.1 μm. The first set of polystyrene

microspheres had a diameter of 1.1 μm with a standard deviation of 0.019 μm. The microspheres had a surface charge density of 12.5 $\mu C/cm^2$, and the density of the polystyrene at 20ºC was 1.055 g/cm^3. The concentration of the batch was 5.5 x 10^{10} particles per mL of latex, and this concentration was diluted to 1.1 x 10^7 particles per mL of latex before the experiments began.

The second set of polystyrene particles had a diameter of 0.51 μm with a standard deviation of 0.010 μm. These microspheres had a surface charge density of 12.0 $\mu C/cm^2$. The initial concentration of the batch was 5.5 x 10^{11} particles per mL of latex, but this was diluted to 1.1 x 10^8 particles per mL of latex for experimentation.

The final set of microspheres had the smallest diameter of 0.12 μm with a standard deviation of 0.014 μm. The surface charge density on the microspheres was 1.8 $\mu C/cm^2$ and had an initial batch concentration of 4.4 x 10^{13} particles per mL of latex which was diluted to 7.04 x 10^{10} particles per mL of latex prior to being used for experimentation. Table 1 shows the parameters for each batch of microspheres.

Table 1: Parameters for Carboxyl Polystyrene Latex Particles

Batch #	Mean diameter (μm)	Standard Deviation of diameter(μm)	Surface Charge Density ($\mu C/cm^2$)	Concentration as Received (particles/mL of latex) x 10^9	Concentration Used in Exps. (particles/mL of latex) x 10^6
1	1.1	0.019	12.5	55	11
2	0.51	0.010	12.0	550	110
3	0.12	0.014	1.8	44000	70400

Colloid concentration and optical density

The colloid concentration was measured with optical density using a spectrophotometer. A sample of approximately 4 mL of colloids at a measured concentration was transferred to a clear, disposable cuvette with the dimensions 45 mm x 12.5 mm x 12.5 mm. A blank sample of approximately 4 mL of deionized water was first

used to zero the spectrophotometer. The cuvette containing the colloids was then placed in the spectrophotometer where the optical density was measured at a wavelength of 650 nm for batches one and two, and at 500 nm for batch 3. These wavelengths were selected because they produced the highest optical density reading for each batch of the polystyrene latex particles.

Five point standard curves were used. Figure 1 shows the strong positive correlation between colloid concentration and optical density and the particle concentration increases linearly as a function of the optical density measured by the spectrophotometer.

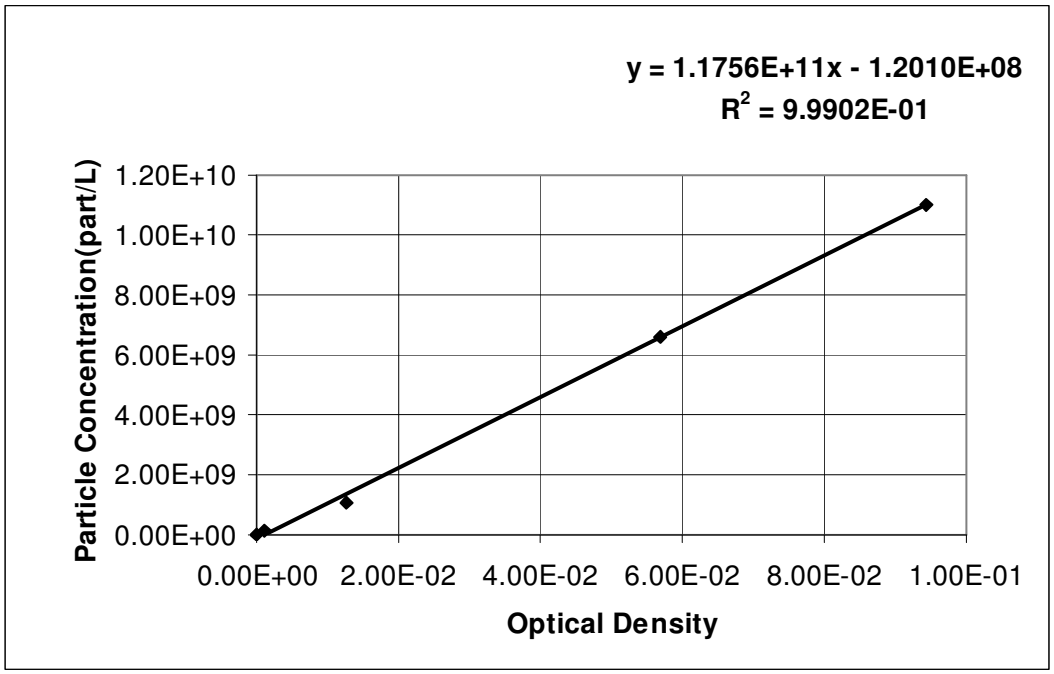

Figure 1: Colloid concentration as a function of the optical density for Batch 1 measured by the spectrophotometer at a wavelength of 650nm

Measurement and Adjustment of pH

The pH of a solution used for attachment or detachment had to be adjusted and measured accurately. Hydrochloric acid and sodium hydroxide were used to reduce and increase the pH respectively. There were two concentrations of HCl and NaOH used

depending on the size of pH adjustment. For larger reductions in pH, concentrated HCl (37.3 %, Fisher Scientific, Pittsburgh, PA) was used, while a diluted HCl solution (approximately 4.7 %, made from concentrated HCl) was used for the smaller reductions in pH. Similarly, a 5 N solution of NaOH (made from 97 % NaOH pellets, Mallinckrodt Chemical Works, St. Louis, MO, New York, NY) was used for the larger increases in pH while a further diluted solution of 0.5 N NaOH (made from 97 % NaOH pellets, Mallinckrodt Chemical Works, St. Louis, MO, New York, NY) was used for the smaller increases in pH.

The pH was measured using a model 720A pH meter (Orion Research Inc, Boston, MA) with a Thermo Orion combination pH probe (Orion Research Inc, Boston, MA). The pH meter was calibrated each day using three buffer solutions having a pH of 4.01, 7.00, and 10.01. The probe was stored in the buffer with a pH of 4.01 each night and rinsed with deionized water before and after each pH measurement. Each pH measurement was made using an identical method to ensure accuracy. The probe was removed from the buffer solution having a pH of 4.01, rinsed with deionized water, and then placed into the flask containing the solution. The probe rested in the middle of the solution for approximately two minutes while a slow swirling motion was made with the flask. After two minutes, the digital pH measurement stopped fluctuating and the pH was recorded. The probe was rinsed with deionized water and stored back in the 4.01 pH buffer solution.

EXPERIMENTAL PROCEDURE

Experimental Setup

The experimental equipment was constructed as shown in Figure 2. The influent passed from the erlenmeyer flask through low density polyethylene (LDPE) tubing which had an OD of 1/8" and an ID of 5/64" (Cole-Parmer, Vernon Hills, IL). The LDPE tubing was connected to the Masterflex L/S 25 pump tubing which had an ID of 0.19" (Cole-Parmer, Vernon Hills, IL). The LDPE tubing was inserted into the wider pump tubing and clamped together. The Masterflex easy-load pump head, model 7518-00 (Cole Parmer, Vernon Hills, IL), was used to pump the solution through the column. At the outlet of the pump, the wider pump tubing was connected to the smaller diameter LDPE tubing by using a plastic clamp as it was done before entering the pump. The pump calibration curve is shown in Figure 3.

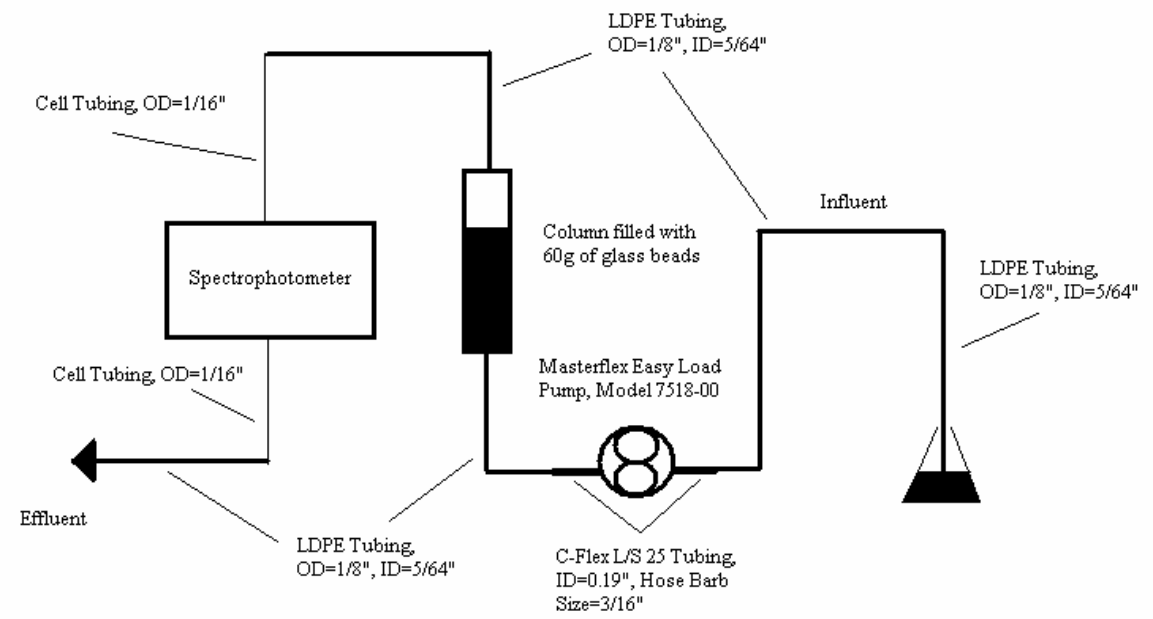

Figure 2: Experimental Apparatus including tubing materials and sizes

The solution was pumped into the glass column (Ace Glass Incorporated, Vineland, NJ) which had a length and inner diameter of 100 mm and 25 mm respectively. The LDPE tubing was attached to a polypropylene male pipe adapter with an OD of 1/8" and a NPT of 1/8" (Cole Parmer, Vernon Hills, IL) affixed to a nylon reducing bushing

with a male NPT of 1/4" and a female NPT of 1/8" (Cole Parmer, Vernon Hills, IL). The reducing bushing was attached to the column which developed a tight seal. The glass beads filled approximately 2/3 of the glass column. The stream exited at the top of the column where the fitting setup was identical to that at the bottom of the column. Before the stream entered the spectrophotometer cell, a Teflon PFA[3] reducing union with an OD of 1/8" and 1/16" (Cole Parmer, Vernon Hills, IL) was used to attach the LDPE tubing to the smaller cell tubing. The stream passed through the cell in the spectrophotometer (Varian Cary 50 Scan UV-Visible Spectrophotometer, Varian Australia PTY LTD, Australia) where an optical density reading was measured at a predetermined wavelength. The stream exited the spectrophotometer and passed through the effluent cell tubing. A Teflon PFA[3] reducing bushing, identical to that at the inlet of the spectrophotometer, was used to attach the cell tubing to the larger effluent stream LDPE tubing. The effluent was collected in an erlenmeyer flask.

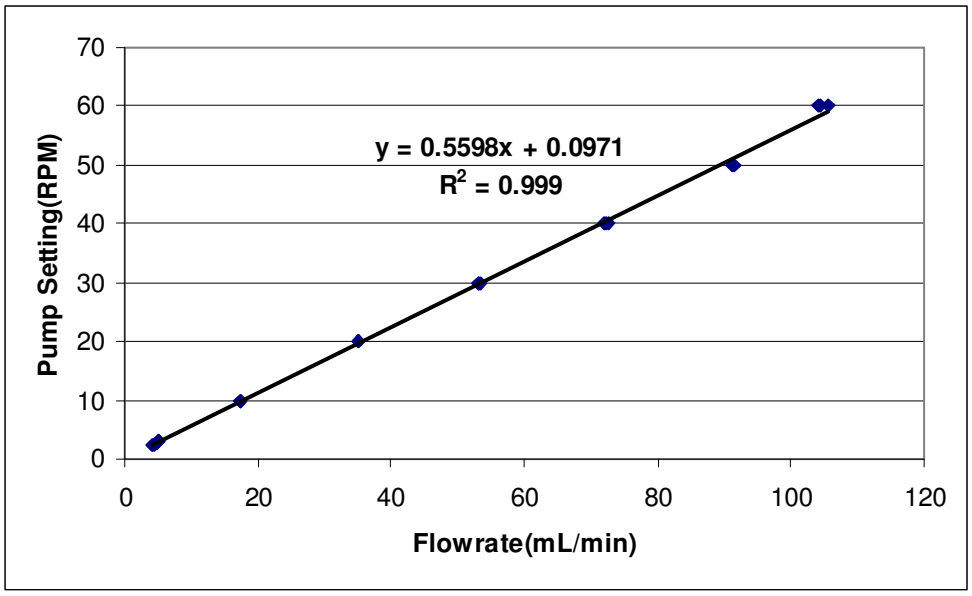

Figure 3: Pump calibration curve for determining RPM setting for a desired flowrate using a Masterflex model 7518-00 pump head and Masterflex 0.19" ID L/S 25 tubing

Attachment

The particles were attached using a solution with a pH of 4.5 ± 0.05 along with an ionic strength (I) of 0.01 M, favorable conditions for attachment. The attachment step was done at a constant flowrate of 5 mL/min. The particles in solution were sonicated for 2 minutes immediately prior to the attachment process in order to break up any weak aggregates which may have formed. Before the attachment step, 10 pore volumes or 140 mL of particle free solution with a pH of 4.5 ± 0.05 and an ionic strength of 0.01 M was pumped through the column at a rate of 5 mL/min to remove any air from within the column and to adjust the solution chemistry in the column to the desired conditions. The attachment step was performed using 20 pore volumes of particle containing solution with a pH of 4.5 ± 0.05 and an ionic strength of 0.01 M at a constant flowrate. The concentration of the particles in the attachment solution depended on the batch and size of the latex particles used. For each size and batch of latex particles, a concentration versus optical density plot was developed prior to any attachment/detachment experimentation. The 20 pore volumes of particle containing attachment solution were followed by 10 more pore volumes of a particle free solution of the same pH and ionic strength at the same flowrate. The flushing solution removed any particles that were not attached to the porous glass media leaving behind only those particles which were successfully attached.

The particle containing solution was mixed with sodium chloride as the electrolyte. The colloids, which were previously sonicated for 2 minutes, were added to the solution using a pipet to reach the desired concentration. The solution was sonicated for another 2 minutes. Before attaching the particles, the original optical density, Co, was

measured. The wavelength of the spectrophotometer was set to 650 nm for particle batches one and two and to 500 nm for batch 3, and zeroed using a cuvette containing approximately 4 mL of deionized water. A sample of 4 mL of the particle containing solution was then placed into a cuvette and inserted into the spectrophotometer where a measurement of the Co was recorded. The Co was used in determining the actual number of particles which attached to the porous glass media.

Throughout the attachment and detachment runs, the spectrophotometer was set to continuously record optical density measurements every 0.5 seconds for 200-400 minutes (depending on the detachment experiment duration) at a constant wavelength of either 650 nm or 500 nm depending on the particles used. All data was saved as a spreadsheet ascii file to be later analyzed using Sigmaplot.

Detachment

Flowrate Perturbations: After the polystyrene latex microspheres had been attached to the glass bead media in the glass column, the flowrate of the influent solution was increased in order to promote detachment. However, the influent solution chemistry was first changed to either a pH of 6 or 8 and an ionic strength of either 0.01 M or 1.0 mM to represent possible conditions in an actual system and to promote detachment. The detachment experiments were labeled and identified based on the solution chemistry of the detachment solution**.** Table 2 shows the four detachment solutions used in experiments involving flowrate perturbations.

The detachment solution was pumped through the column at increasing flowrates with each flow duration lasting 25 pore volumes. The flowrate was initially identical to the attachment flowrate of 5 mL/min and then increased to 25, 50, 75, and 100 mL/min,

pump settings of 14.1, 28.1, 42.1, and 56.1 RPM respectively. Each flowrate of detachment solution was held constant for 25 pore volumes and the spectrophotometer measured the amount of detachment which occurred due to each change in flowrate. A final rinse with a solution having a pH of 11.0 and an ionic strength of $10^{-5.5}$ M (deionized water) was used to remove more of the remaining attached particles. After the final rinse, the operation was complete and the data was saved. In order to remove the remaining attached particles, the column was fluidized with approximately 30 pore volumes of a solution with a pH of 11.0 and an ionic strength of $10^{-5.5}$ M (DI). Figure 4 shows the detachment curve for particles with a diameter of 1100 nm using a detachment solution with a pH of 8.0 and an ionic strength of 0.01 M.

Table 2: Detachment solutions used in experiments with flowrate perturbations

Detachment Solution	pH	Ionic Strength
M4	6.0	0.01 M
M5	8.0	0.01 M
M6	6.0	0.001 M
M7	8.0	0.001 M

Solution Chemistry Perturbations: The particles were attached at a pH of 4.5 and an ionic strength of 0.01 M operating at a flowrate of 5 mL/min. The particles were then detached by keeping the flowrate and ionic strength constant and increasing the pH of the influent solution. Each solution of increasing pH was pumped through the system for 20 pore volumes. For example, in the first case, with a constant ionic strength of 0.01 M, the solution pH was increased to 7.0, 9.0, and 10.0. A final rinse was pumped through the column using DI at a pH of 11.0 at the same constant flowrate.

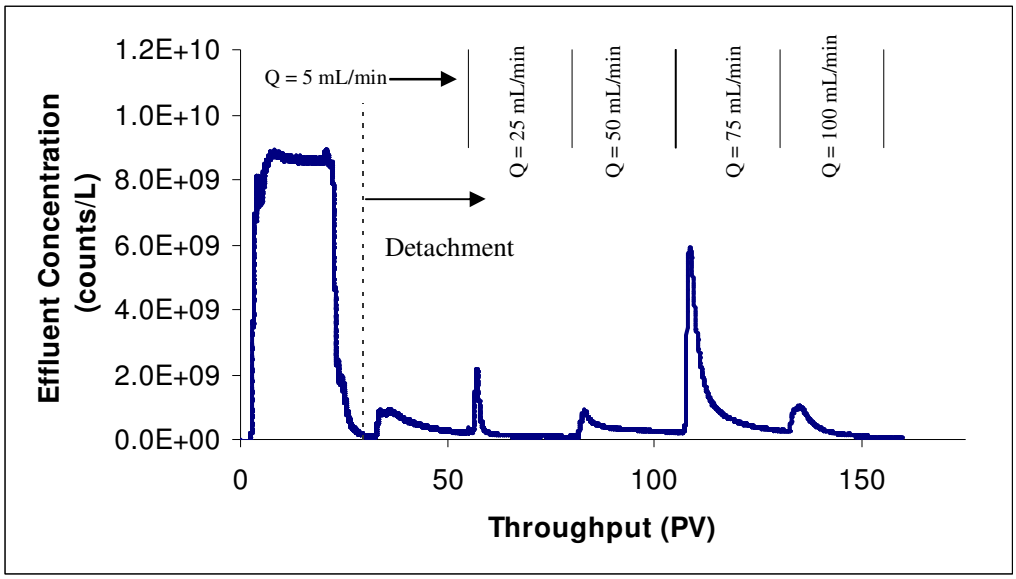

Figure 4: Results for a typical attachment and detachment curve: particles are attached for 20 pore volumes at a pH of 4.5 and I = 0.01 M, flushed with an identical solution for 10 pore volumes, then detached in this case under M5 conditions which include a pH of 8.0 and I = 0.01 M with each flow being pumped through the packed bed for 25 pore volumes

The optical density of the effluent was measured at a constant wavelength of 650 nm or 500 nm, depending on the particles used, throughout the process of increasing the pH to measure the magnitude of detachment. This process of increasing the pH was performed for two different constant ionic strengths. In the second scenario, the ionic strength of the detachment solution was held constant at 1mM. After the attachment process, the influent tubing was placed in a flask containing a solution with a pH of 4.5 and an ionic strength of 1mM. The solution was pumped through the column for 20 pore volumes. The process then followed with increasing increments of pH as done in the first case with the (I) remaining constant at 1mM and the flowrate remaining constant at 5 mL/min.

RESULTS AND DISCUSSION

Surface Roughness

The roughness parameter of concern for determining particle detachment was the peak to peak distance (λ). For both batches of chemically etched glass beads, this λ parameter became the significant measurement for the difference in surface roughness. Table 3 shows values for the three roughness parameters and the fraction of detachment measured for a minimum shear of 100.6 s^{-1} using a solution with a pH of 6.0 and ionic strength of 0.01 M (M4Z conditions).

Table 3: Roughness parameters and measured detachment using a solution with M4Z conditions

Roughness Parameter	Chromic-12 95% C.I. (nm)	CA/AF 95% C.I. (nm)	
RMS1	269.082 - 171.757	358.460 - 204.182	
RMS2	197.612 - 102.644	170.133 - 107.980	
P-V Heights1	1157.855 - 743.436	1105.103 - 746.332	
P-V Heights2	89.878-151.752	91.963-159.434	
λ1	644.696 - 457.492	1005.225 - 641.027	
λ2	64.964 - 50.084	60.136 - 47.622	
Frac.Detach @ 100.6 s^{-1}	0.4600	0.3414	d = 1.10 μm
Frac.Detach @ 100.6 s^{-1}	0.4250	0.3528	d = 0.51 μm
Frac.Detach @ 100.6 s^{-1}	0.1769	0.2600	d = 0.12 μm

A two sample T-test with unequal variances was used to statistically measure the significance of the RMS and P/V heights for the two batches. Based on the two-tailed P values in the T-test, the hypothesis which stated RMS_1, RMS_2, $(P/V)_1$ height, and $(P/V)_2$ height were equal for both batches couldn't be shown to be not true based on a 95% confidence interval. The trends for λ_1 and λ_2 with detachment in Table 3 show the significance of the peak to peak distance. For particles with diameters of 1100 nm and 510 nm, more detachment occurred from beads chemically etched using the chromic acid procedure. The λ_1 for beads etched with chromic acid was much less than that for beads

etched with the citric acid/ammonium fluoride solution. The trend shows λ_1 is the controlling roughness parameter on detachment of particles with diameters of 1100 nm and 510 nm.

For particles with a diameter of 120 nm, the opposite detachment trends were measured. Greater detachment occurred from beads chemically etched with the citric acid/ammonium fluoride solution. The measured detachment can be explained by the trends of the secondary roughness parameter, λ_2. The λ_2 for beads chemically etched with chromic acid is larger than the λ_2 for beads chemically etched with the citric acid/ammonium fluoride. The trend shows that the controlling roughness parameter on detachment for particles with a diameter of 120 nm is λ_2.

The λ_1 parameter was a measurement for the larger scale overall surface peak to peak roughness, while the λ_2 parameter was a measurement for the smaller scale peak to peak roughness. The mean λ_1 and λ_2 values for the beads etched using the citric acid/ammonium fluoride solution were 823.1 nm and 53.9 nm respectively. Similarly, the mean λ_1 and λ_2 values for the beads etched using chromic acid were 551.1 nm and 57.5 nm respectively.

For experiments where the larger colloids (1100 nm and 510 nm in diameter) were detached, the determining factor was λ_1, but for the smallest particles of 120 nm, the secondary λ_2 became the major parameter. The particle diameter to λ ratios can be used to evaluate the significance of both the λ_1 and λ_2 parameters on the three particle sizes. Table 4 shows the three particle sizes along with the d/λ_1 and d/λ_2 ratios for both batches of chemically etched glass beads. For the largest particles with a diameter of 1100 nm, the d/λ_1 values for glass beads etched using citric acid/ammonium fluoride and chromic

acid are 1.34 and 2.00 respectively. The d/λ_2values are much larger at 20.41 and 19.13 for the beads etched using citric acid/ammonium fluoride and chromic acid respectively. The d/λ_1 values are closer to unity (a value of 1.0) than the d/λ_2 values meaning the particle diameter and λ_1 values are much closer in scale than the particle diameter and λ_2 values. Based on this analysis and the trends from Table 3, the λ_1 parameter proves to be the significant factor when discussing detachment of particles having a diameter of 1100 nm.

Table 4: The d/λ_1 and d/λ_2 ratios for each of the three particle sizes and each batch of chemically etched glass beads

Particle Diameter(nm)	Citric Acid/Ammonium Fluoride		Chromic Acid	
	d/λ_1	d/λ_2	d/λ_1	d/λ_2
1100	1.34	20.41	2.00	19.13
510	0.62	9.46	0.93	8.87
120	0.15	2.23	0.22	2.09

Similar to the behavior of the particles with a diameter of 1100 nm, the λ_1 parameter proves to be the significant factor in analyzing the detachment of particles with a diameter of 510 nm. For particles with a diameter of 510 nm, the d/λ_1 values for beads etched with citric acid/ammonium fluoride and chromic acid are 0.62 and 0.93 respectively. The d/λ_2 values for the two batches of glass beads are 9.46 and 8.87 respectively. As for the largest particles, the d/λ_1 values are closer to unity than the d/λ_2 values. The λ_1 parameter is the controlling roughness parameter when dealing with the detachment of particles with a diameter of 510 nm.

In the case of the particles with a diameter of 120 nm, the d/λ_1 values for beads etched with citric acid/ammonium fluoride and chromic acid are 0.15 and 0.22 respectively. However, the d/λ_2 values are 2.23 and 2.09 respectively for the two batches

of glass beads. Unlike the previous two cases, the d/λ_2 values are closer to unity than the d/λ_1 values meaning that the particle diameter and λ_2 values are much closer in scale than the particle diameter and λ_1 values. For particles with a diameter of 120 nm, the controlling roughness factor proves to be the λ_2 parameter.

Qualitative Detachment for Hydrodynamic Shear

A qualitative analysis was developed to evaluate the detachment of particles from the media surface. The analysis focused on the cumulative fraction of detachment which occurred at a flowrate of 75 mL/min. For each particle size, there were a total of four trials, each having a unique detachment solution. For a given particle size, it was expected that there would be less detachment as the λ-value increased. Therefore, it was expected that there would be less detachment as the d/λ-value decreased and more detachment as d/λ increased.

Figure 5 shows the cumulative fraction of particles detached at a flowrate of 75 mL/min as a function of the d/λ parameter. Figure 5 displays detachment for all four trials and a regression line for each of the three particle sizes. For particles with a diameter of 1100 nm and 510 nm, $\lambda = \lambda_1$, but for particles with a diameter of 120 nm, $\lambda = \lambda_2$. The d/λ values are normalized with the lower of the two values set to 1.0. In the case where $\lambda = \lambda_1$, the higher λ-value is associated with the beads that were chemically etched using the citric acid/ammonium fluoride solution. This means that the d/λ values for the beads etched using the citric acid/ammonium fluoride solution were the lower of the two and were normalized to a value of 1.0. In the case where $\lambda = \lambda_2$, the higher λ-value represented the beads that were chemically roughened using the chromic acid solution. This means that the d/λ values for the beads etched using the chromic acid were lower

and were set to a value of 1.0. The data was normalized in order to display it all on a single plot in Figure 6.

The detachment results support the expected trends. For each particle size in Figure 5, there is an increase in the cumulative fraction of particles detached as the d/λ-value increases. The slope of the regression line is shown on each plot only to give a value to the positive trend between particles detached and the d/λ-value. The R^2 value for particles with a diameter of 1100 nm is 0.9043 showing a strong positive correlation between the data. The R^2 values drop to 0.7232 and 0.5516 for particles with diameters of 120 nm and 510 nm respectively. Although these correlations are not as strong as for the 1100 nm particles, the focus of the analysis was to show the positive trend between the fraction of particles detached and the d/λ-value. In all three cases, there is a clear increase in cumulative fraction of particles detached for an increase in the d/λ-value. Figure 6 shows the same qualitative analysis, but displays the data for all three particle sizes on one plot. In order to completely understand particle detachment and the effect of roughness of the media surface, a mathematical model incorporating roughness must be developed.

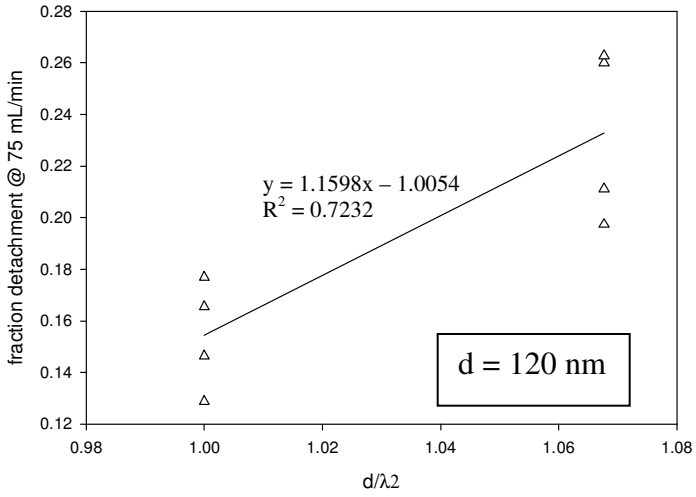

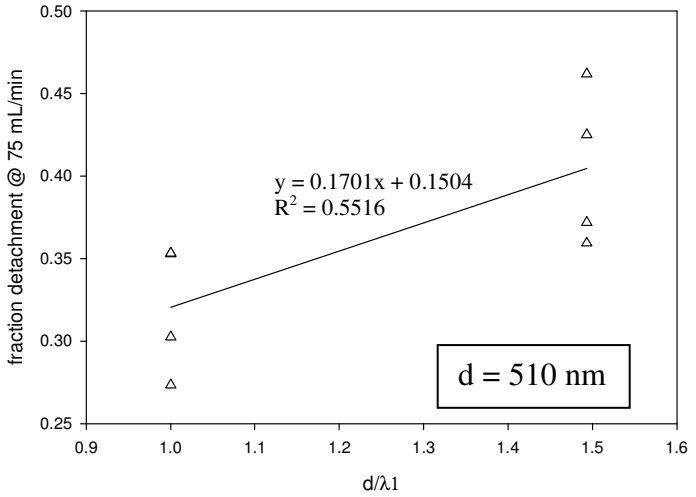

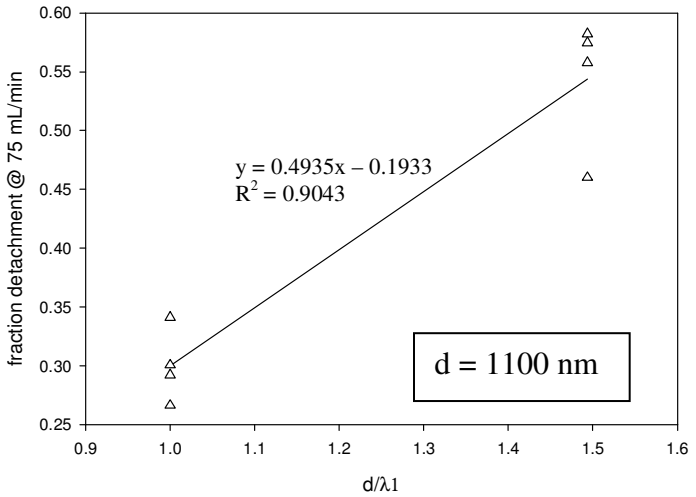

Figure 5: Fraction of particles detached at a flowrate of 75 mL/min as a function of d/λ where $\lambda = \lambda_1$ for particles with a diameter of 1100 nm or 510 nm and $\lambda = \lambda_2$ for particles with a diameter of 120 nm

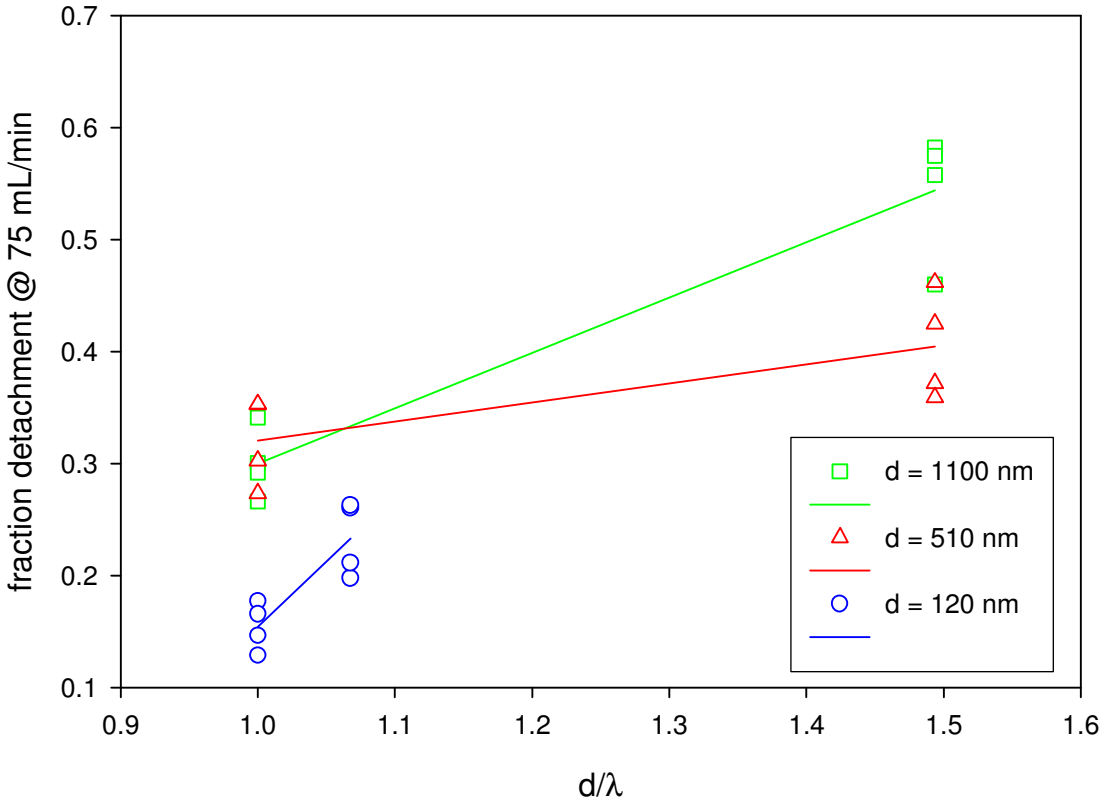

Figure 6: Fraction of particles detached at a flowrate of 75 mL/min as a function of d/λ and normalized such that the lower d/λ value is set to 1.0, where $\lambda = \lambda_1$ for particles with d = 1100 nm and 510 nm and $\lambda = \lambda_2$ for particles with d = 120 nm

Moment Balance

After the attachment solution has been passed through the column and the flushing solution has removed any particles which were not attached to the media surface, the detachment solution is pumped through the column. During detachment, there are three forces acting on the particle. These three forces are the drag force (F_d), lift force (F_L), and the force of adhesion (F_{ad}). Figure 7 displays an attached particle contacting a rough surface at two points and the three forces acting on it. Assuming the forces act on the center of the particle, the moment balance on the attached particle around the downstream point of contact is represented by Equation 3.

$$\mathbf{F_{ad}(X) = F_d(Z) + F_L(X)} \qquad \mathbf{(3)}$$

The X-value and Z-value represent the horizontal and vertical distances respectively from the center of the particle to the downstream point of contact. Upon detachment, the particle will rotate around the downstream point of contact. The moment balance is essential in determining the minimum required shear to remove an attached particle from the media surface.

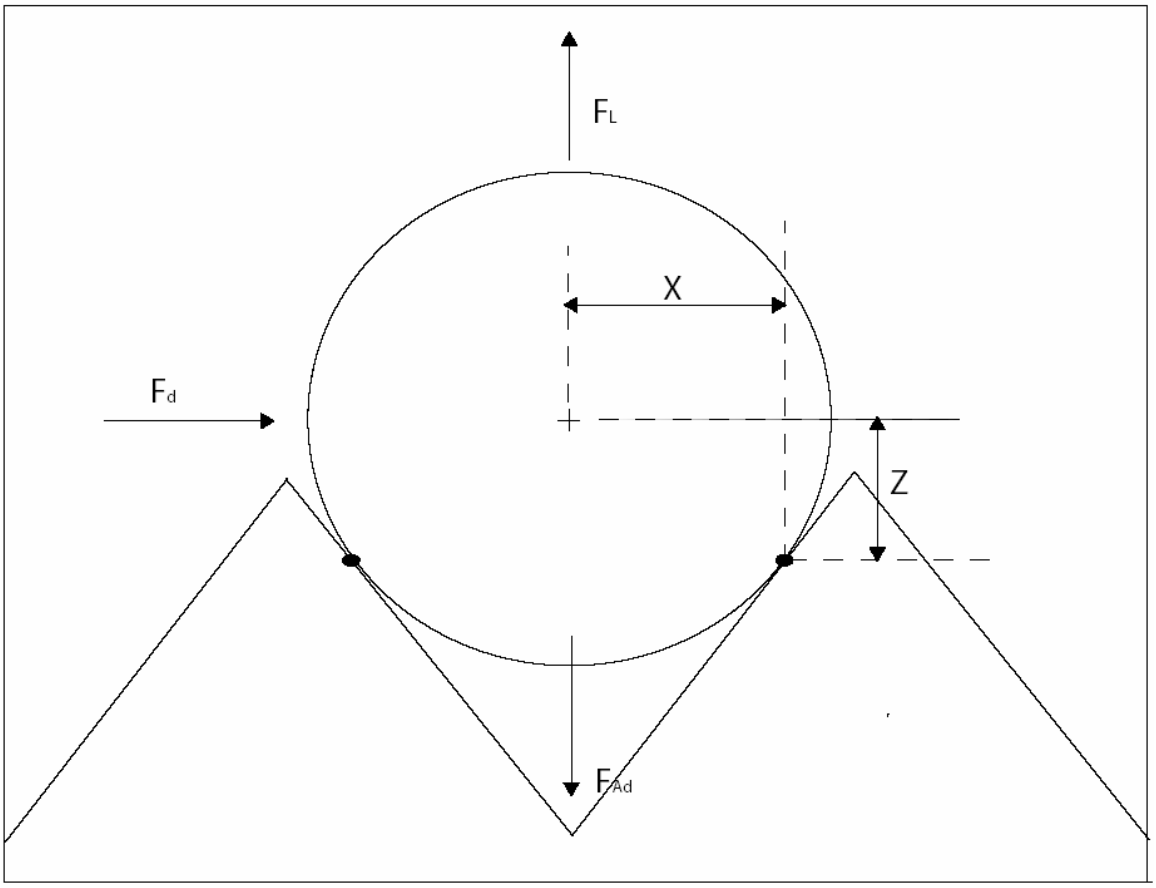

Figure 7: Attached particle and the three forces acting on it during detachment

The values for X and Z must be determined in order to perform the moment balance. Two distinct cases develop when determining the values for X and Z. In the first case, the particle contacts the media surface at two points within the "valley" as shown in Figure 7. The dimensions, parameters, and mathematical relationships used in determining the X and Z values for the initial case are illustrated in Figure 8. The point at the base of the valley in which the particle is attached is set as the origin, (0,0), using

the rectangular coordinate system. The angle θ is calculated using Equation 4, where H is the P/V height and λ is the peak to peak distance.

$$\theta = \arctan[(\lambda/2)/H] \quad (4)$$

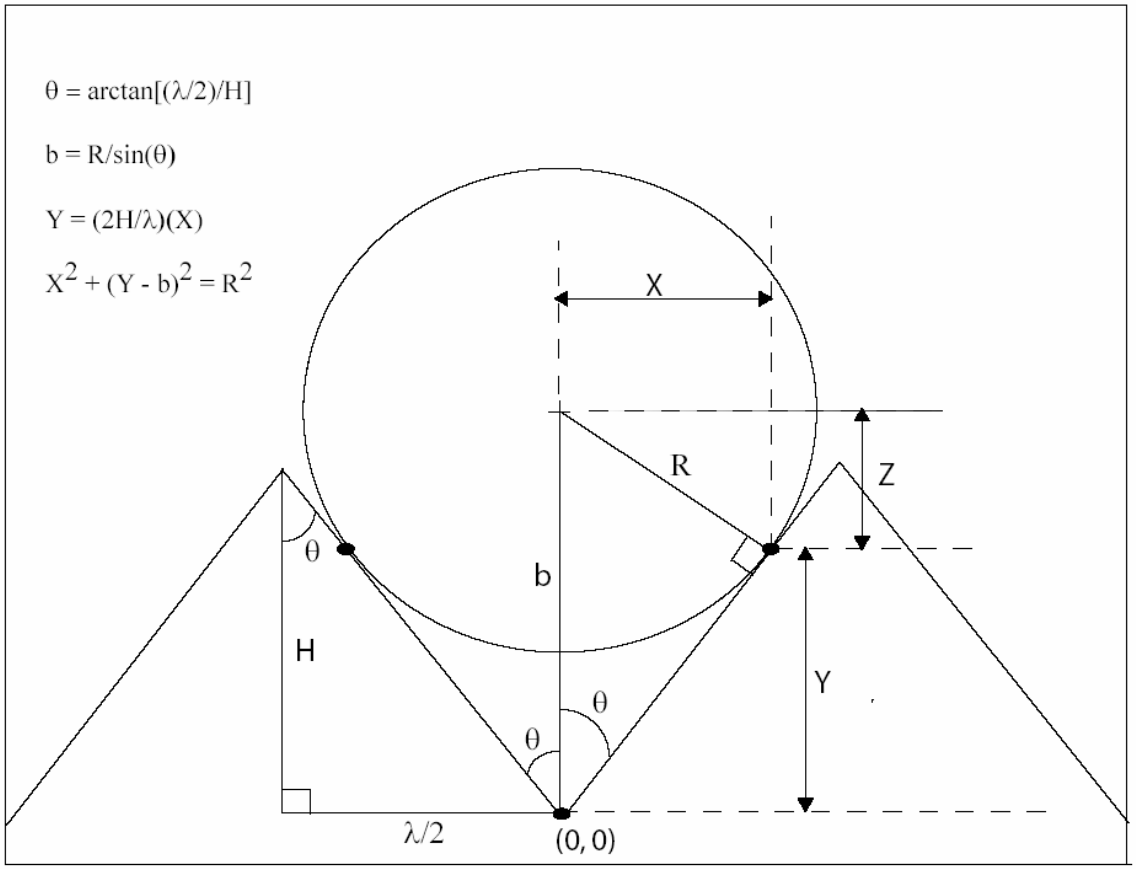

Figure 8: Dimensions, parameters, and mathematical relationships used in determining the X and Z values for analyzing the moment balance when the particle is attached within the "valley"

The angle θ and the radius of the particle, R, are used in Equation 5 to determine the b-value.

$$b = R/\sin(\theta) \quad (5)$$

The b-value represents the distance from the bottom of the valley of the media surface to the center of the attached particle. The radius intersects the media surface line which must be tangent to the spherical particle. This forms a right angle which allows Equation 5 and the trigonometric relationship in it valid. With the b-value known, a series of two

equations with two unknowns can be developed. Equation 6 represents the line starting at the origin and tangent to the attached particle.

$$\mathbf{Y = [(2H/\lambda)]X} \quad \mathbf{(6)}$$

Equation 7 represents the surface of the spherical particle, where the center of the particle is located at the coordinate point (0, b).

$$\mathbf{X^2 + (Y - b)^2 = R^2} \quad \mathbf{(7)}$$

spherical particle, where the center of the particle is located at the coordinate point (0, b). The system of equations can be solved by substituting Equation 6 into Equation 7, solving for the X-value, and then using the X-value to solve for the Y-value. Equation 8 is used to determine the Z-value, the final unknown parameter required to complete the moment balance.

$$\mathbf{Z = b - Y} \quad \mathbf{(8)}$$

The mathematical relationships for finding X and Z become simplified when the particle is attached at the two peaks of the media surface Figure 9 illustrates a particle which contacts the media surface at the two peaks rather than within the valley. The parameters, dimensions, and simplified mathematical relationships used in finding the X and Z-values are included in Figure 9. Based on Figure 9, the X-value can be determined using Equation 9.

$$\mathbf{X = \lambda/2} \quad \mathbf{(9)}$$

With the X-value and the radius, R, of the attached particle, the Pythagorean Theorem is used to calculate the Z-value in Equation 10.

$$\mathbf{Z^2 = R^2 - X^2} \quad \mathbf{(10)}$$

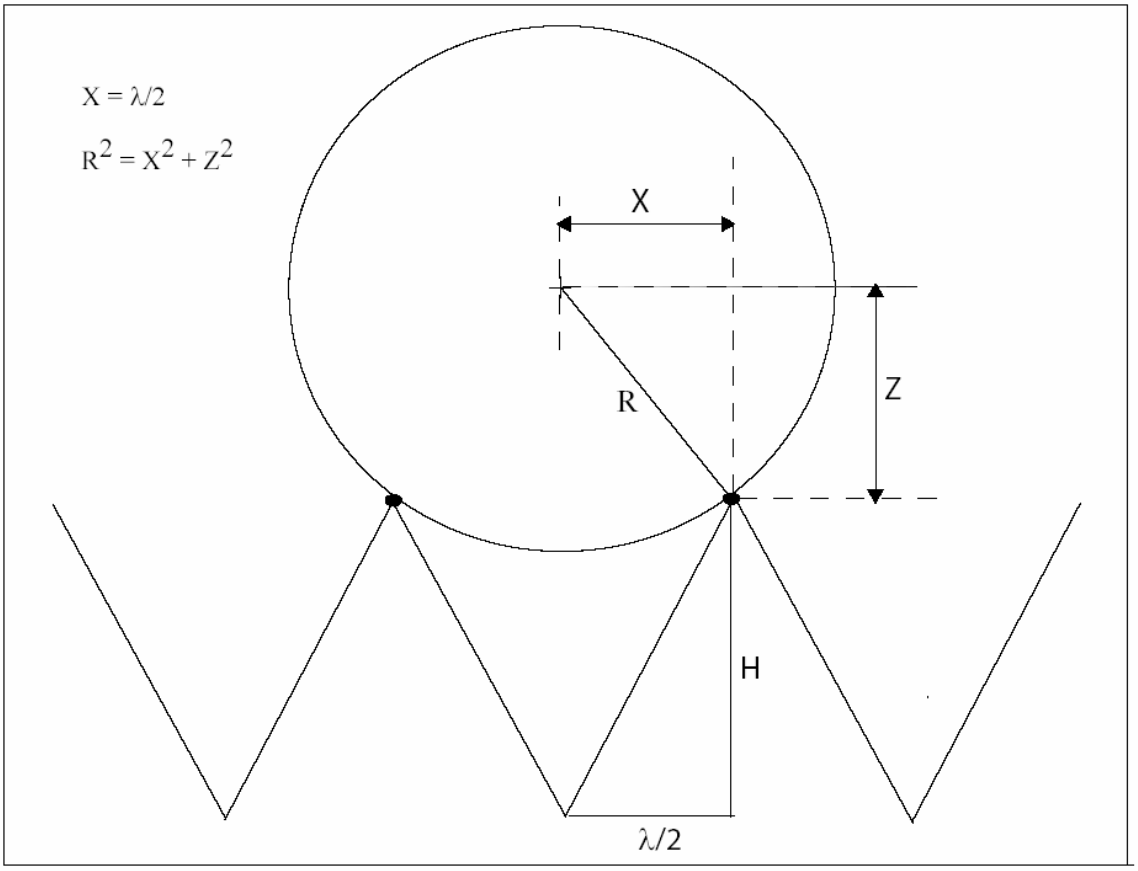

Figure 9: Dimensions, parameters, and mathematical relationships used in determining the X and Z-values when the particle is attached at the two peaks of the media surface

The X and Z-values are used to perform the moment balance in Equation 4. The moment balance is used to determine the minimum shear required to roll and remove an attached particle from the media surface. The force of adhesion (F_{Ad}) must be determined before the minimum required shear for detachment can be calculated. The force of adhesion is estimated using Equation 3. With the X and Z-values previously determined, the drag force and lift force must be defined. The drag force (F_d) is defined using Equation 11 (Bergendahl and Grasso, 1998), where μ is the dynamic viscosity of water at 25°C (8.998×10^{-4} N-s/m^2) and S is the fluid shear passing through the porous media bed within the column.

$$\mathbf{F_d = 10.205 \cdot \pi \cdot \mu \cdot S \cdot R^2} \qquad \mathbf{(11)}$$

Equation 11 represents the drag force experienced by a spherical particle attached to a smooth media surface. When attached to a smooth surface, the entire cross sectional area of the particle is exposed to the fluid flow. However, in the case where the media surface has been chemically etched, the fraction of area exposed to the fluid flow decreases based on the roughness of the media surface and the particle diameter. Equation 12 incorporates the fraction of exposed area (f_A) for determining the drag force on an attached particle.

$$\mathbf{F_d = 10.205 \cdot f_A \cdot \pi \cdot \mu \cdot S \cdot R^2} \qquad \mathbf{(12)}$$

The fraction of exposed area is estimated based on two situations. In the first situation the center of the spherical particle (b) is located above the P/V height (H) and the fraction of exposed area is greater than 0.50. Figure 10 shows a particle with its center above the P/V height and the mathematical expressions used in determining the fraction of exposed area. The concealed area in Figure 10 is the area below the two points of contact. The angle associated with the concealed area (δ) is estimated using Equation 13.

$$\mathbf{\cos(\delta/2) = (b - H)/R} \qquad \mathbf{(13)}$$

The angle δ is subtracted from the total angle of a circle, 2π radians, in Equation 14 to determine the angle associated with the exposed area (γ).

$$\mathbf{\gamma = 2\pi - \delta} \qquad \mathbf{(14)}$$

The angle γ is used in Equation 15 to determine the exposed area above the P/V height (Mays, 2001).

$$\mathbf{A_e = 1/8 \cdot (\gamma - \sin(\gamma)) \cdot d^2} \qquad \mathbf{(15)}$$

The fraction of exposed area is calculated using Equation 16, where $\pi d^2/4$ represents the total cross-sectional area of the spherical particle.

$$f_A = A_e/(\pi d^2/4) \quad (16)$$

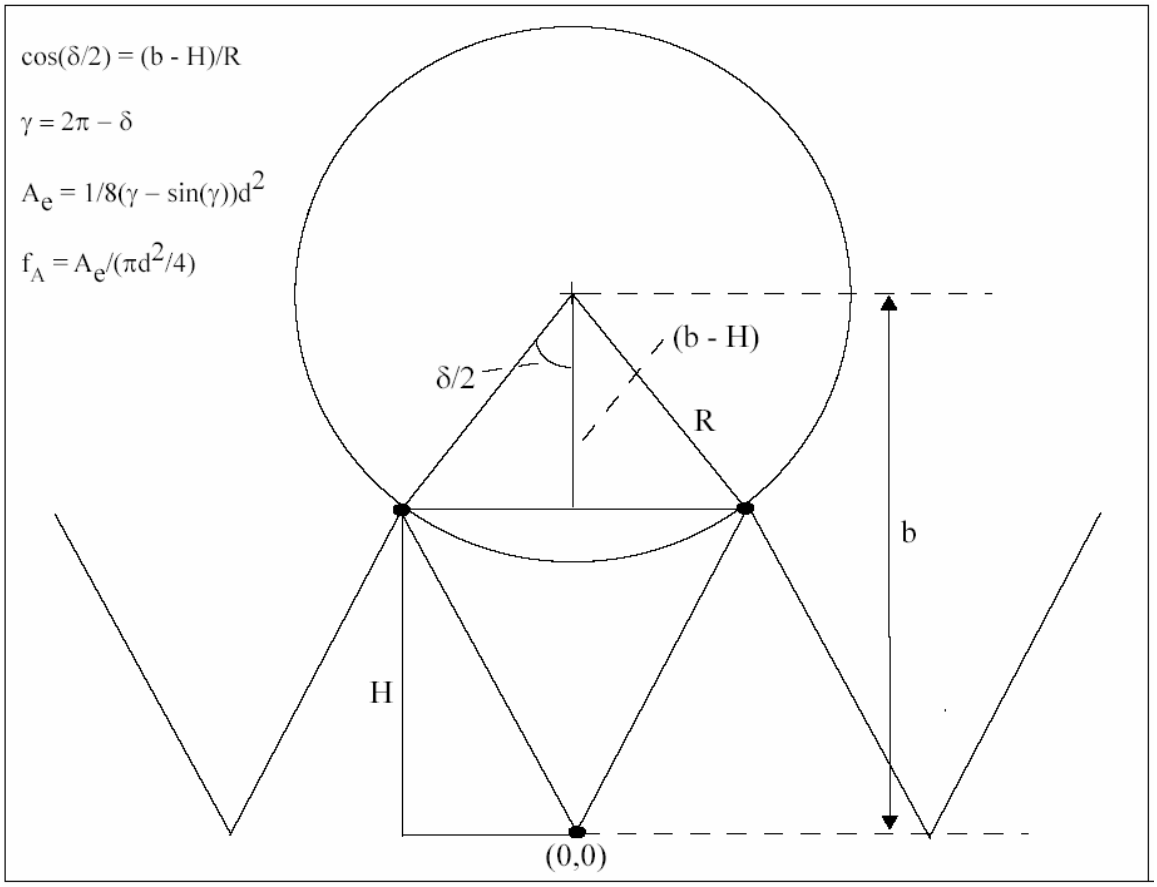

Figure 10: Spherical particle with its center located above the P/V height and the mathematical expressions used to determine the fraction of exposed area above the two points of contact

In the second situation, the center of the particle is located below the P/V height, and the fraction of area exposed to fluid flow is less than 0.50. Figure 11 illustrates a particle with its center located below the P/V height and the mathematical relationships used to determine the fraction of exposed area. In this case, the angle associated with the exposed area, γ, can be estimated using Equation 17.

$$\cos(\gamma/2) = (H - b)/R \quad (17)$$

As done in the prior analysis, Equations 15 and 16 are then used to determine the actual fraction of exposed area for this scenario.

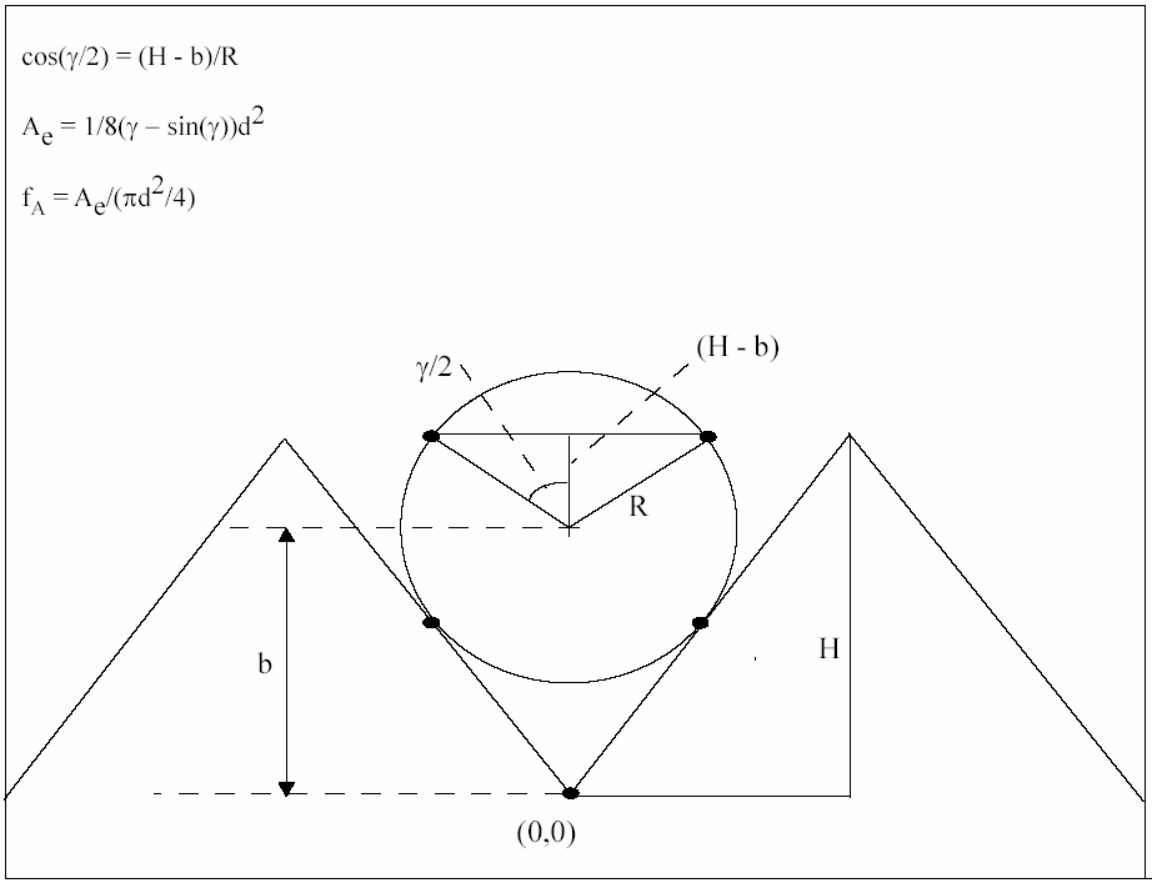

Figure 11: Spherical particle with its center located below the P/V height and the mathematical expressions used to determine the fraction of exposed area above the P/V height

The lift force, F_L, can be estimated using Equation 18 (Bergendahl and Grasso, 1998), where ν is the kinematic viscosity of water at 25°C (9.025 x 10^7 m^2/s).

$$\mathbf{F_L = 81.2 \cdot \mu \cdot R^3 \cdot S^{3/2}/v^{1/2}} \qquad \mathbf{(18)}$$

The minimum fluid shear through the packed column at 75 mL/min is assumed to be 100.6 s^{-1} (Bergendahl and Grasso, 2000).

The column detachment experiments showed that particles with a diameter of 1100 nm experienced approximately 50% detachment at a flowrate of 75 mL/min when attached to media that was chemically etched using the chromic acid procedure. For X and Z-values of 275.547 nm and 475.998 nm respectively, and a fluid shear of 100.6 s^{-1},

Equation 3 was used to determine the force of adhesion for particles with a diameter of 1100 nm (1.4854×10^{-12} N).

However, the force of adhesion is not constant and changes with particle diameter based on the extended-DLVO theory (Bergendahl and Grasso, 1999). The total interaction energy between particles and media surfaces, ΔG^{Σ}, is expressed in Equation 19 (Bergendahl and Grasso, 1999) as the sum of the electrostatic (ΔG^{EL}), van der Waals (ΔG^{VDW}), Born repulsion (ΔG^{Born}), and Lewis acid-base (ΔG^{AB}) interaction energies.

$$\mathbf{\Delta G^{\Sigma} = \Delta G^{EL} + \Delta G^{VDW} + \Delta G^{Born} + \Delta G^{AB}} \qquad \mathbf{(19)}$$

Based on the linear superposition approximation (LSA), a prediction for the electrostatic interaction energy for dissimilar surfaces can be made. Values for the electrostatic interaction energy that are estimated by the LSA equation are between the range of those determined from electrostatic equations based on constant charge and constant potential assumptions (Elimelech et al., 1995). Equation 20 (Gregory, 1975) represents the sphere-plate LSA equation used to determine the electrostatic interaction energy between the colloid and media surface,

$$\Delta G^{EL} = 64\pi\varepsilon R\left(\frac{kT}{z_j e}\right)^2 \gamma_1\gamma_2 \exp(-\kappa s) \qquad \mathbf{(20)}$$

where:

$$\gamma_i = \tanh\left(\frac{z_j e \psi_{o,i}}{4kT}\right) \qquad \text{and} \qquad \kappa = \sqrt{\frac{e^2 \Sigma n_{jo} z_j^2}{\varepsilon kT}}$$

The difference in size scale of the particles and the porous media allows for the sphere-plate geometry to be used. Equation 21 (Gregory, 1981) predicts the retarded van der Waals interaction energy.

$$\Delta G^{VDW} = -\frac{A_{132} \cdot R}{6 \cdot s}\left[1 - \frac{5.32 \cdot s}{\lambda}\ln\left(1 + \frac{\lambda}{5.32 \cdot s}\right)\right] \quad \textbf{(21)}$$

The Born repulsion interaction energy is determined using Equation 22 (Ruckenstein and Prieve, 1976).

$$\Delta G = \frac{A \cdot \sigma_c^6}{7{,}560}\left[\frac{8R + s}{(2R + 7)^7} + \frac{6R - s}{s^7}\right] \quad \textbf{(22)}$$

The collision diameter (σ_c) in Equation 22 was varied to achieve a primary minimum depth at 0.158 nm which is a commonly accepted distance of closest approach d_o (van Oss, 1994). The Lewis acid-base interaction energy is estimated using Equation 23 (van Oss, 1994).

$$\Delta G^{AB} = 2\pi R \lambda_{AB} \Delta G_{do}^{AB} \exp\left[\frac{d_o - s}{\lambda_{AB}}\right] \quad \textbf{(23)}$$

Equation 23 demonstrates that the interaction energy between the particle and media surface decays exponentially as a function of distance. The extended DLVO-theory is used to predict the change in interaction energy due to varying particle diameter. The interaction energy is directly proportional to the force of adhesion, and thus the extended DLVO-theory predicts the change in the force of adhesion as a function of particle diameter. The interaction energy and the Langbein approximation for the interaction area are used in Equation 24 to determine the interaction energy per unit area (W) (Israelachvili, 1992).

$$\mathbf{W = \Delta G_{min}/(2 \cdot \pi \cdot R \cdot d_o)} \quad \textbf{(24)}$$

The interaction energy per unit area is used in the JKR model, Equation 25 (Johnson, Kendall, and Roberts, 1971), to estimate the force of adhesion.

$$\mathbf{F_{ad} = 3/2 \cdot \pi \cdot W \cdot R} \quad \textbf{(25)}$$

Figure 12 shows the linear relationship between the adhesion force and the particle diameter. However, the actual values for the adhesion force shown in Figure 12 are those represented by the interaction energy between the particles and a flat, smooth surface. The extended DLVO theory is only used to determine the effect of changing particle diameter on the adhesion force relative to that for particles of 1100 nm. As shown in Figure 12, there is a direct linear correlation between the particle diameter and the adhesion force. Based on the adhesion force of 1.4854×10^{-12} N determined for particles with a diameter of 1100 nm and the direct linear relationship between particle size and adhesion, Equation 26 is developed to estimate the adhesion force for any given particle size.

$$F_{ad} = \frac{d}{1100}(1.4854 \times 10^{-12}) \qquad \textbf{(26)}$$

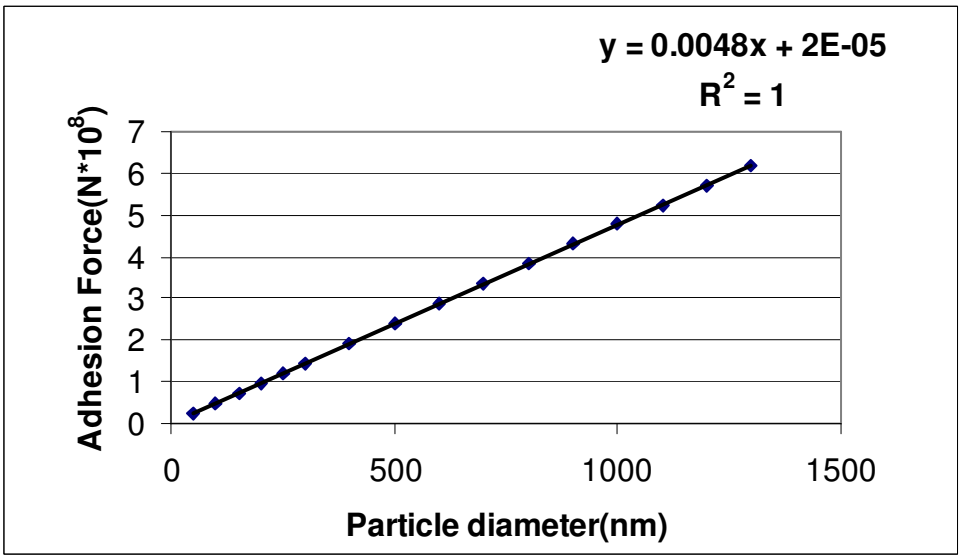

Figure 12: Adhesion force as a function of particle diameter based on the JKR model and extended DLVO theory

The overall focus of performing the moment balance around the point of contact between the attached particle and the media surface is to determine values for the minimum fluid shear required to remove the attached particles from the media surfaces.

The analysis begins with assigning a fluid shear of 100.6 s^{-1} to the experimental data set where the particles had a diameter of 1100 nm and the media was chemically etched using the chromic acid procedure. The force of adhesion is determined for particles with a diameter of 1100 nm and then used in Equation 26 to determine the force of adhesion for any given particle diameter. The force of adhesion along with the X and Z-values are then used in Equation 3 to estimate the minimum fluid shear required to detach the particles. The X and Z-values are dependent on the particle diameter and the roughness of the media surface, which consists of both the λ-value and the P/V height. A parametric study showing the change in minimum fluid shear required for detachment as a function of surface roughness was performed.

Parametric Study

The parametric study investigated the effect of the particle diameter and the media surface roughness (λ-value and P/V height) on the minimum fluid shear required to detach the attached particles. The three parameters were varied in order to show the change in minimum fluid shear. The first part of the parametric study used values for particle diameter ranging from 1300 nm to 300 nm which decrease by increments of 200 nm. The media λ-values range from 300 nm to 1300 nm and increase by increments of 100 nm. The study was done for two P/V heights including 1000 nm and 500 nm. This first parametric study represents primary roughness conditions where the λ_1-value and $(P/V)_1$ height are the significant variables in considering surface roughness. A second part of the parametric study was done looking at the effect of secondary roughness where the λ_2-value and $(P/V)_2$ height were the significant variables. The particle diameter was varied from 50 nm to 250 nm increasing by increments of 50 nm, and the λ-value ranged

from 50 nm to 250 nm increasing by increments of 50 nm. The (P/V) height was held constant at 100 nm. In both parts of the parametric study the fraction of particle area exposed to fluid flow was limited to greater than 0.50. Conditions which caused the center of the particle to lie below the (P/V) height (fraction of exposed area less than 0.50) were not considered. The mechanism for detachment with particles having a fraction of exposed area less than 0.50 may involve parameters and factors which need further investigation.

For each set of conditions in the parametric study, the minimum fluid shear required for detachment was determined. Bergendahl and Grasso (2000) used a similar experimental setup and determined the constricted tube model was the best representation of the void space between spherical media in a packed column. According to the constricted tube model, the minimum fluid shear through a pore in the packed bed due to a fluid flowrate of 75 mL/min is approximately 100.6 s^{-1}.

The results of the model with P/V height held constant at 1000 nm are shown in Figure 13. The model shows that the shear required for detachment increased as λ increased. The shear required for detachment for particles with diameters of 1300 nm, 1100 nm, and 900 nm is below 100 s^{-1} for media with a λ-value of 300 nm. With a peak to peak distance of 300 nm on the media surface, these particles are attached to the peaks of the surface. As λ is increased, meaning the peak to peak distance becomes further apart, the particle moves further into the "valley" although still attached to the peaks. This causes a reduction in the fraction of exposed area, an increase in X, and a decrease in Z. These are the three parameters which work simultaneously to either increase or decrease the shear required for detachment as roughness changes. In the scenario where

λ increases, the changes in each of the three parameters all contribute to an increase in shear. Thus, an increase in the fraction of exposed area, a decrease in the X-value, or an increase in the Z-value contributes to reducing the shear required for detachment.

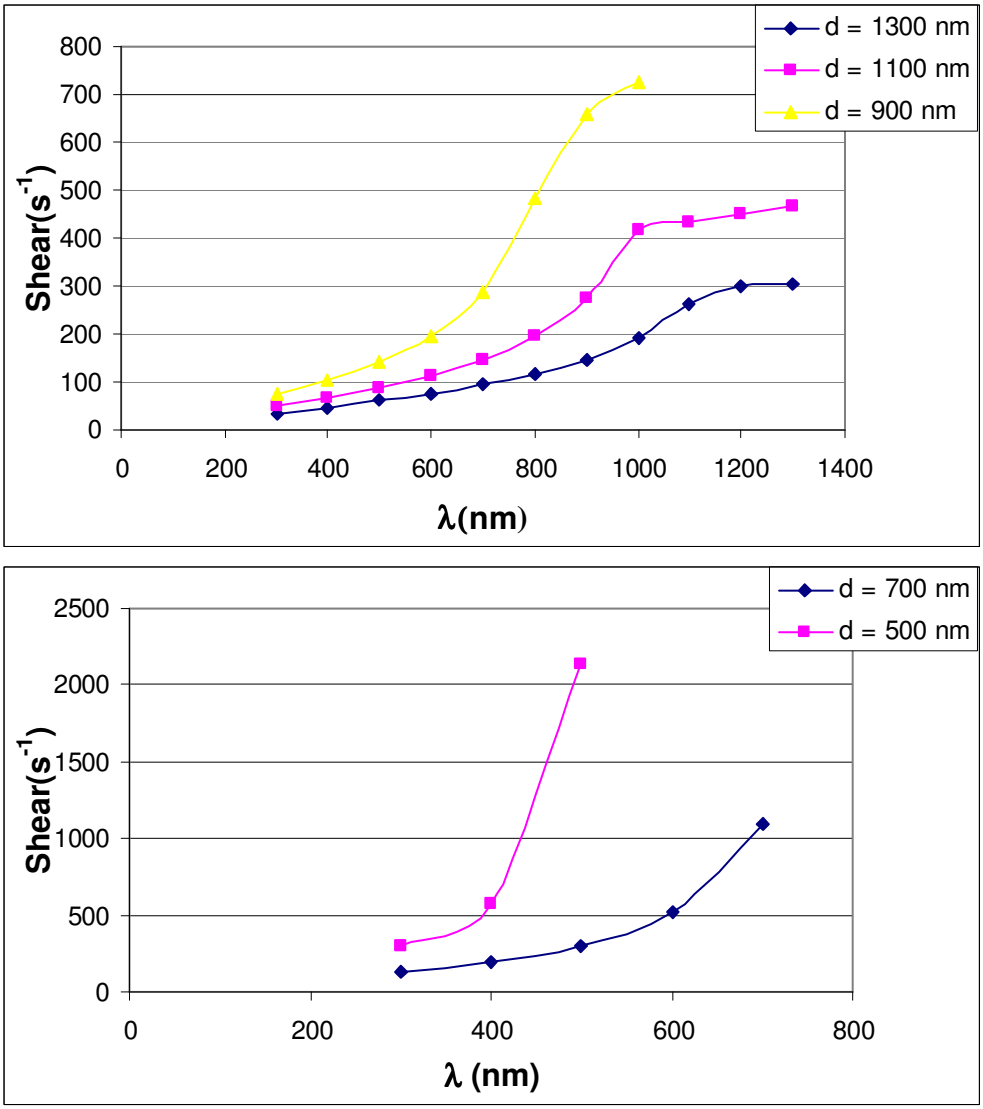

Figure 13: Shear required to achieve particle detachment as a function of λ for a constant P/V height of 1000 nm

In this first case where the P/V height is constant at 1000 nm, there is a point on the curves representing particles a diameters of 1300 nm and 1100 nm where the slope appears to approach zero. The λ-values where the slope begins to approach zero for particles with a diameter of 1300 nm and 1100 nm are approximately 1200 nm and 1000

nm respectively. At these λ-values, the particle was no longer attached to the peaks of the media surface, but rather penetrated into the "valley" where it became attached to two points below the peaks. The curve begins to level off as a result of the change in the fraction of exposed area, the X-value, and the Z-value. When the particle was attached to the peaks of the valley of the media surface, the increasing λ-value caused all three parameters to change in a manner which causes an increase in shear requirement. However, when the particle penetrates into the valley and becomes attached to the surface within this valley, an increase in the λ-value no longer changes the three parameters in such a way that they all contribute to an increase in shear requirement. As the λ-value increases, the fraction of exposed area continues to decrease which still contributes to an increase in required shear. The X-value decreases and the Z-value increases which both contribute to a decrease in the required shear. In this case where the P/V height is large at 1000 nm, the increase in required shear due the decreasing exposed area is slightly larger than the decrease in required shear due to the changing X and Z-values. Therefore, the overall shear requirement still continues to increase although at a minimal rate as the λ-value increases. As an example, an increase in the λ-value beyond the value of 1200 nm for particles with a diameter of 1300 nm causes only a minor increase in the required shear for 50% detachment compared to previous identical increments of increases in the λ-value.

The shear requirements for particles with diameters of 1300 nm and 1100 nm when attached to a media surface with a λ of 1300 nm are 302.6 s^{-1} and 468.1 s^{-1}. For particles with a diameter of 900 nm, the largest value for shear occurs at a λ of 1000 nm and equals 725.6 s^{-1}. The fraction of exposed area for particles with a diameter of 900

nm attached to a media surface with a λ of 1100 nm or greater is below 0.5. The shear requirement is not estimated for particles with a fraction of exposed area less than 0.5. The total number of data points for particles with a diameter of 700 nm and 500 nm decreases compared to the larger particles. This is due to the fraction of exposed area dropping below 0.5 at smaller λ-values for these smaller particles. The largest shear requirements for particles with a diameter of 700 nm and 500 nm occur at 700 nm and 500 nm respectively. At λ-values greater than these, the fraction of exposed area drops below 0.5 and the data points are not determined. The largest shear requirement for particles with diameters of 700 nm and 500 nm are 1098.0 s^{-1} and 2135.9 s^{-1} respectively.

The shear present in the pores of the porous media may increase to more than twice that present at the widest part of the pore based on the constricted tube model. The constricted tube model is an idealistic model that makes several assumptions. The model assumes ideal conditions including smooth surfaces and uniform, identical, parabolically shaped pore spaces. However, with the media chemically etched, the pore spaces formed by these no longer smooth, spherical beads vary throughout the column. This causes the pore velocity of the fluid and the shear produced by the fluid flow through the pores to vary more than that previously determined by the constricted tube model. There are pore spaces within the packed bed where the shear developed is below the 100.6 s^{-1} and above the shear at the pore throats predicted by the constricted tube model to be 980.8 s^{-1}. These shear values found by the detachment model of 1098.0 s^{-1} and even 2135.9 s^{-1} may be present in localized areas within the packed bed.

The results of the model for a P/V height of 500 nm are similar to those at a P/V height of 1000 nm. Figure 14 shows the shear required for detachment as a function of

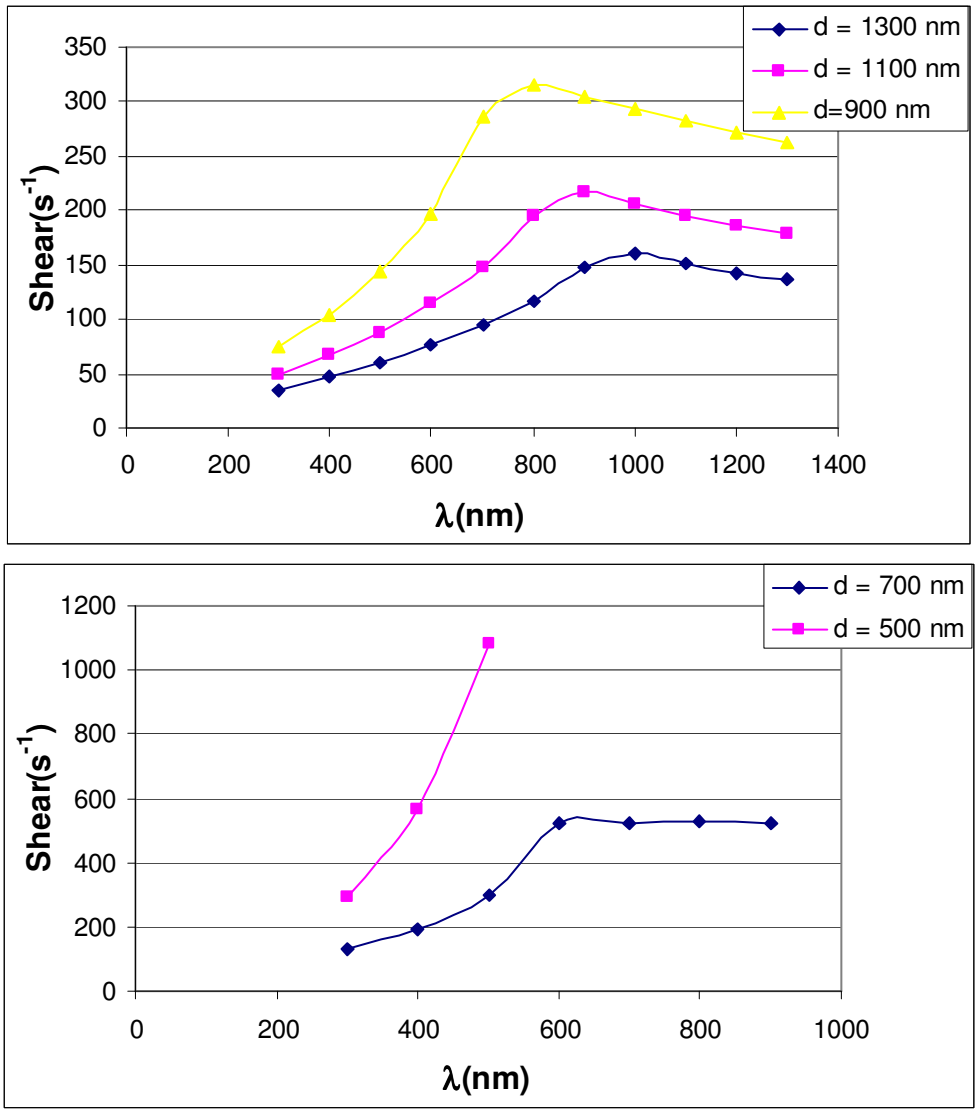

Figure 14: Shear required for detachment as a function of λ for a constant P/V height of 500 nm

the λ-value for a constant P/V height of 500 nm. The shear requirements are identical to those for a constant P/V height of 1000 nm when the particle is attached to the peaks of the valley. However, for particles with diameters of 1300 nm, 1100 nm, and 900 nm, the particle begins to attach to the surface within the valley at a lower λ-value than it does for a constant P/V height of 1000nm. For example, at a P/V height of 1000 nm, particles with a diameter of 1300 nm begin to attach to the media surface within the valley at a λ-value of 1200 nm. When the P/V height is 500 nm, particles with a diameter of 1300 nm

begin to attach to the surface within the valley at a λ-value of 1000 nm. When the particle begins to attach to the surface within the valley, the shear requirements begin to differ significantly for P/V heights of 1000 nm and 500 nm.

The point where the particle begins to penetrate the valley and attach to the surface within the valley is represented by the peak of the curves in Figure 14. After this point of initial penetration, the shear requirement decreases as the λ-value is increased. For a P/V height of 1000 nm, the normalized shear requirement continued to slightly increase after this point, but this is not the case with a constant P/V height of 500 nm. As discussed when the P/V height was 1000 nm, the three parameters affecting the shear required for detachment are the fraction of exposed area and the X and Z-values. For λ-value increases beyond this initial point of valley penetration, the fraction of exposed area decreases contributing to an increase in the shear requirement. Similar to the P/V height of 1000 nm, at a P/V height of 500 nm, the X-value decreases and the Z-value increases for an increase in λ-value which both contribute to a decrease in the shear requirement. However, the magnitude of the decrease in shear requirement due to the change in X and Z-values is greater than the magnitude of the increase in shear requirement due to the decrease in the fraction of exposed area. The overall result is a decrease in the shear requirement as the λ-value increases beyond the point of initial particle attachment within the valley of the media surface.

Figure 15 shows the shear required for detachment as a function of the λ-value for a constant P/V height of 500 nm for only particles with a diameter of 1100 nm. An illustration is displayed corresponding to each of the three positions where the particle is attached to the media surface. The first phase represents an increasing shear requirement

for an increasing λ-value which corresponds to the particle being attached at the peaks of the valley. The second phase occurs at the peak of the shear requirement curve where the particle first begins to attach to the surface within the valley. The third phase is represented by the decreasing shear requirement where the particle attaches to the media surface well within the valley. This third phase is similar to the third phase when the P/V height is constant at 1000 nm. The difference between the two as discussed previously is that at a P/V height of 500 nm, the fraction of exposed area remains much greater than that when the P/V height is 1000 nm.

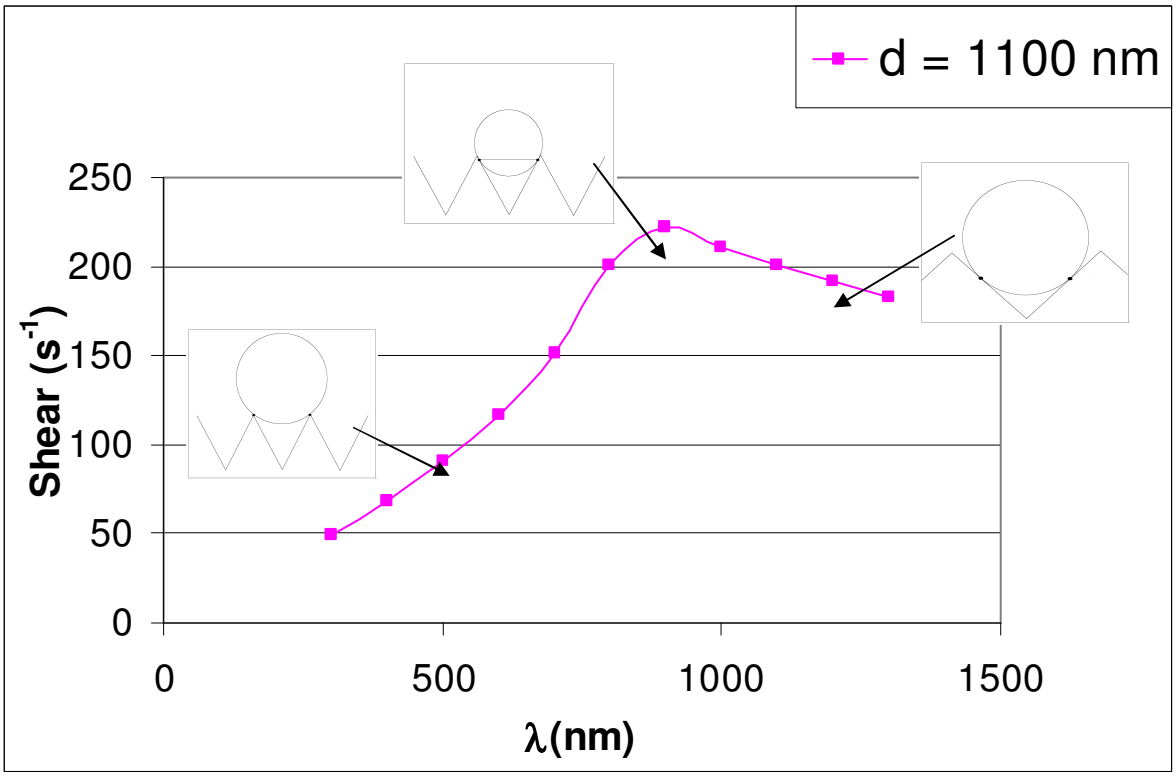

Figure 15: Shear required for detachment as a function of λ for a constant P/V height of 500 nm while illustrating the particle position in regards to the attachment points on the media surface

At a P/V height of 1000 nm, the particle falls deeper into the valley leaving a smaller fraction of exposed area, larger X-value, and smaller Z-value than that produced by the same size particle attached to the media surface with a P/V height of 500 nm.

These parameters cause the difference in the change in shear requirement for increases in the λ-value. At a P/V height of 1000 nm, the shear requirement continues to increase while at a P/V height of 500 nm, the shear requirement begins to decrease as a result of increasing the λ-value. The parametric study shows that the shear required for detachment decreases as the P/V height decreases for a constant particle diameter and constant λ-value. At a λ-value of 1200 nm and P/V height of 1000 nm, the shear requirement for detachment for a particle with a diameter of 1300 nm is 299.8 s^{-1}. With the particle size and λ-value constant, the shear requirement for a P/V height of 500 nm drops to less than half of that for a P/V height of 1000 nm at 143.0 s^{-1}.

In the smaller particles, the λ_2-value and the $(P/V)_2$ height became the roughness variables of concern. Figure 16 shows the shear required for detachment as a function of the λ-value for a constant P/V height of 100 nm. The results show identical trends to those for a P/V height of 500 nm. There is an initial increase in shear required for detachment when the particle is attached to the peaks of the media surface. The shear curve reaches a peak where the particle initially attaches to the media surface below the peaks and within the valley. For λ-values greater than the initial penetration point the curve begins to decrease as the particle attaches to the media surface further into the valley. The actual values for the shear requirement in Figure 16 range from a low of 153.0 s^{-1} for particles with a diameter of 250 nm at a λ-value of 50 nm to a high of 2308.9 for particles with a diameter of 150 nm at a λ-value of 150 nm.

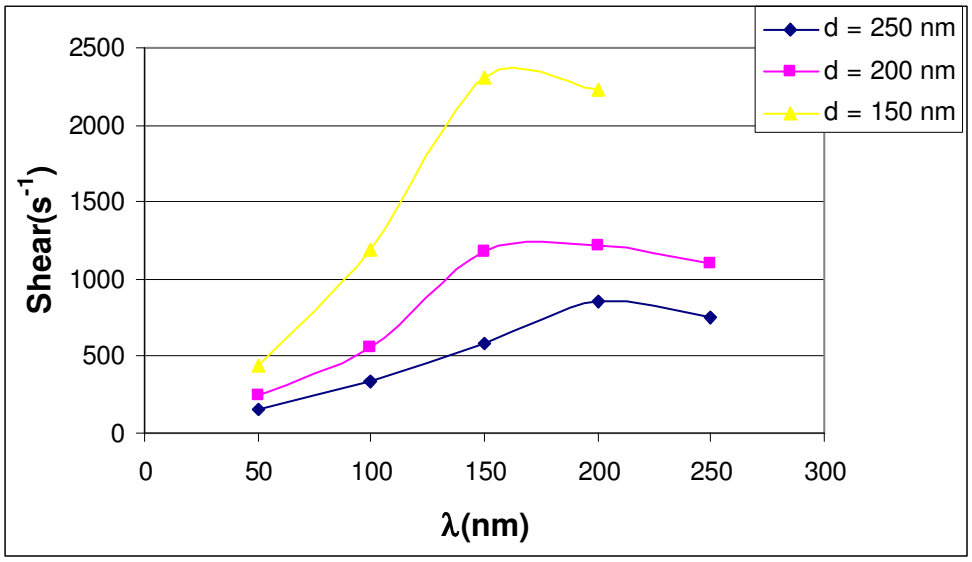

Figure 16: Shear required for detachment as a function of λ for a constant P/V height of 100 nm for particles ranging from 150 nm to 250 nm

Experimental Data Points for Hydrodynamic Shear

The theoretical parametric study has developed a model to predict the shear requirement curves for detachment for various particle diameters, λ-values, and P/V heights. The experimental data collected must be compared to the theoretical curves developed by the study to determine the validity of the model. The first two experimental data points are shown in Figure 17 for particles with a diameter of 1100 nm. The data point at 551.1 nm, data point 1, represents the minimum shear in the packed bed at a flowrate of 75 mL/min. This minimum shear value of 100.6 s^{-1} was used along with particles with a diameter of 1100 nm and media chemically etched using chromic acid as the base point for the parametric study. This point falls exactly on the detachment curve for particles with a diameter of 1100 nm. The values for the fraction of detachment for particles with a diameter of 1100 nm attached to media surfaces chemically etched using the chromic acid method range from 0.45 to 0.58.

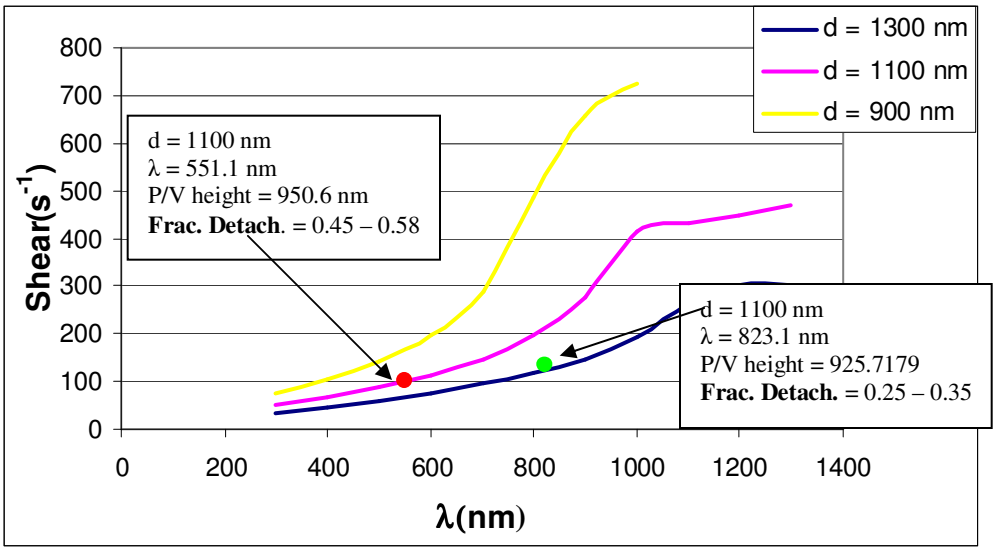

Figure 17: Theoretical shear requirement curves for detachment as a function of λ showing the two experimental data points

The data point at a λ-value of 823.1 nm, data point 2, represents the minimum shear at a flowrate of 100 mL/min of 134.2 s^{-1}. A flowrate of 100 mL/min was the highest experimental flow pumped through the packed bed. The actual experimental detachment due to the minimum shear of 134.2 s^{-1} ranged from 0.41 to 0.48. The model predicts that the actual shear required for detachment of particles with a diameter of 1100 nm for a λ-value of 823.1 nm and P/V height of 925.7 nm is 210.3 s^{-1}. The experimental percent detachment should be and is less than 50% for a flow producing a minimum shear of 134.2 s^{-1}.

The experimental detachment was less than 50% for particles with a diameter of 120 nm. For these smaller particles, the λ_2-value and $(P/V)_2$ height were used in determining the theoretical shear required to achieve detachment. At a λ-value of 53.9 nm and P/V height of 125.7 nm, the predicted shear required for detachment is 798.6 s^{-1}. The greatest flowrate used to detach the particles was again 100 mL/min producing a minimum shear of 134.2 s^{-1}. The experimental range of detachment for these conditions, data point 3, was 0.24 to 0.32 and is represented by the red data point in Figure 18.

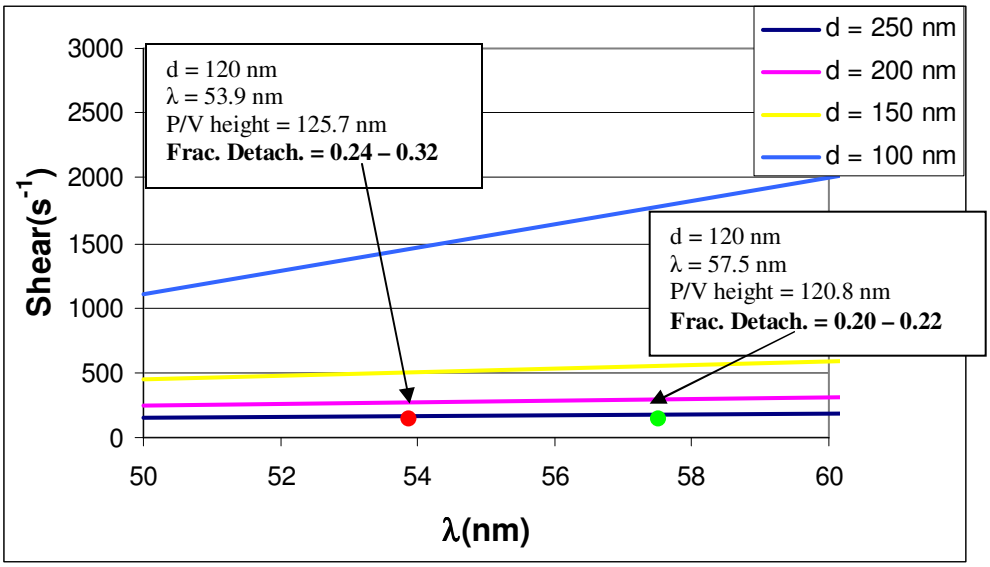

Figure 18: Theoretical shear requirement curves for detachment as a function of λ showing two experimental data points

The second experimental data point in Figure 18, data point 4 (green), represents conditions including a λ-value of 57.5 nm and a P/V height of 120.8 nm. The model predicted a shear for detachment to be 872.0 s^{-1} which is greater than that predicted for the same size particles attached to a media surface with a λ-value 53.9 nm. With the experimental minimum shear remaining 134.2 s^{-1}, the fraction of particle detachment for this fourth experimental data point is expected to be less than that for the first point. The actual fraction of detachment ranged from 0.20 to 0.22 which was expected based on the prediction of the shear predicted by the model to achieve detachment.

The ranges for the fraction of particle detachment for the two experimental data points show similar trends based on the model's prediction for shear requirement. The model predicts a shear requirement for particles attached to a surface with a λ-value of 53.9 nm and a P/V height of 125.7 nm of 798.6 s^{-1}. The shear requirement predicted by the model for these same size particles attached to a surface with a λ-value 57.5 nm and a P/V height of 120.8 nm is 73.4 s^{-1} more at 872.0 s^{-1}. Based on the theoretical shear

requirements, it's expected that less detachment would be achieved for the fourth experimental data point when comparing it to the third. The actual experimental detachment ranges show the expected trend with the third data point having a range of detachment of 0.24 to 0.32 and the fourth having a range of detachment of only 0.20 to 0.22.

The experimental fraction of detachment and the theoretical shear required for 50% detachment for particles with diameters of 1100 nm and 120 nm are shown in Table 5. Table 5 shows three experimental data points experiencing a constant minimum shear of 134.2 s^{-1} and one data point with a smaller minimum shear of 100.6 s^{-1}. In the case where the minimum shear of 100.6 s^{-1} was used, an actual fraction of detachment of approximately 0.50 was achieved. For the other three cases, 50% detachment was not achieved and the greatest flow pumped through the packed bed produced a minimum shear of 134.2 s^{-1}. The trends for particle detachment are clearly shown in Table 5. As the shear requirement for detachment predicted by the model increases, the actual fraction of detachment decreases for a constant minimum shear experienced in the pore spaces. Based on the trends shown in Table 5, it would be expected that for a model shear requirement greater than 872.0 s^{-1}, the actual fraction of particle detachment would be less than 0.20.

The remaining two experimental data points for particles with a diameter of 510 nm are not compared to the theoretical model. The fraction of exposed area when these particles are attached to the glass beads chemically etched using the chromic acid procedure, data point 5, is approximately 0.41. Conditions where the fraction of exposed area was less than 0.50 were not considered by the theoretical model due to the

uncertainty which the role of exposed area takes on the drag force and therefore the shear requirement. In the prior four experimental data points which included the particles with a diameter of 1100 nm and 120 nm, the lowest fraction of exposed area was approximately 0.90 meaning the fraction of exposed area did not have a large effect on the results. However, for data point 5, the fraction of exposed area will play a major role in decreasing the drag force and will therefore cause a large theoretical shear requirement for 50% detachment. If data point five was considered in the model, the shear requirement for detachment would be 2396.6 s^{-1}. Even at this high theoretical shear requirement for 50% detachment, the actual range for the fraction of particle detachment is 0.37 to 0.48 for a minimum shear of 134.2 s^{-1}. Based on the previous four experimental data points, the expected experimental fraction of detachment would be below 0.20.

Table 5: Experimental data points for particles with a diameter of 1100 nm and 120 nm showing the theoretical shear required for 50% detachment predicted by the model, the actual minimum shear developed in the pore spaces, and the actual experimental fraction of detachment achieved in each case

Experimental Data Point	Model Shear for 50% Detachment	Minimum Shear through Pore Spaces	Experimental Fraction of Detachment
1	100.6 s^{-1}	100.6 s^{-1}	0.45 – 0.58
2	210.3 s^{-1}	134.2 s^{-1}	0.41 – 0.48
3	798.6 s^{-1}	134.2 s^{-1}	0.24 – 0.32
4	872.0 s^{-1}	134.2 s^{-1}	0.20 – 0.22

Data point 6 represents conditions where particles with a diameter of 510 nm are attached to the media surface chemically etched using the citric acid/ammonium fluoride solution. Similar to the previous data point, data point 6 is not considered by the theoretical model due to the fraction of exposed area being below 0.5. In this case, the particle is attached deep within the valley producing a fraction of exposed area of zero

and meaning the particle is completely concealed from the fluid flow. This would mean that the expected fraction of particle detachment should be zero. However, the experimental fraction of detachment is 0.33 to 0.40 showing that the fraction of exposed area takes a different role than that defined by the model for particles with a fraction of exposed area greater than 0.50.

In comparison to the same size particles attached to the media surface chemically etched using the chromic acid (data point 5), the fraction of particles detached for data point 6 is less. This means that the trend of less detachment achieved when identical particles are attached to media surfaces with higher λ-values holds true even for these particles not considered by the model. However, the experimental values for the actual fraction of particles detached does not fall within the expected range based on the theoretical model and the experimental fractions of detachment for the first four data points. The reason for the discrepancy must be the inaccurate usage of the fraction of exposed area in Equation 13 when the value for the fraction of exposed area decreases further from a value of unity of 1.0.

Experimental Detachment with Solution Chemistry Changes

Colloid detachment due to changing solution chemistry was measured for the two batches of chemically etched glass beads. Particles were attached and detached at a constant flowrate of 5 mL/min. Solutions of increasing pH at a constant ionic strength were used to detach the attached colloids. Figure 19 shows the fraction of detachment due to increasing the pH for particles with a diameter of 1100 nm at a constant ionic strength of 0.01 M and 0.001 M. Figure 19 shows less detachment occurs from the rougher beads with a greater λ. The trend of less detachment with a greater λ may be

explained by the van der Waals attraction force. At a greater λ, the particles attach closer to the center of the media. As the particles move closer to the center of the media, more molecules from both the colloid and the media interact with each other causing an increase in the force of adhesion. The increase in the force of adhesion makes it more difficult for detachment to occur, and the trends shown in Figure 19 were observed.

Similar trends were observed for particles with a diameter of 510 nm. Figure 20 shows the fraction of detachment as a function of pH and ionic strength. The fraction of detachment is less for particles attached to the rougher glass beads which have a greater λ. Similar to the analysis for particles with a diameter of 1100 nm, as λ increases, the colloids attach closer to the media center. Closer attachment increases molecular interactions, van der Waals attraction, and the force of adhesion. Roughness was found to decrease the detachment of particles with diameters of 1100 nm and 510 nm.

For the smallest particles with a diameter of 120 nm, the difference in detachment from one batch of beads to the other was not significant. The overall detachment in both cases was much less than that observed for the two larger particle sizes. The van der Waals attraction may give some explanation as to why there was no difference. The smallest particles attach well within the "valley" on the primary roughness scale. The difference in colloid position and closeness to the media center due to secondary roughness from one batch of beads to the other was not significant, and the difference in the van der Waals attraction between the two batches of beads was negligible.

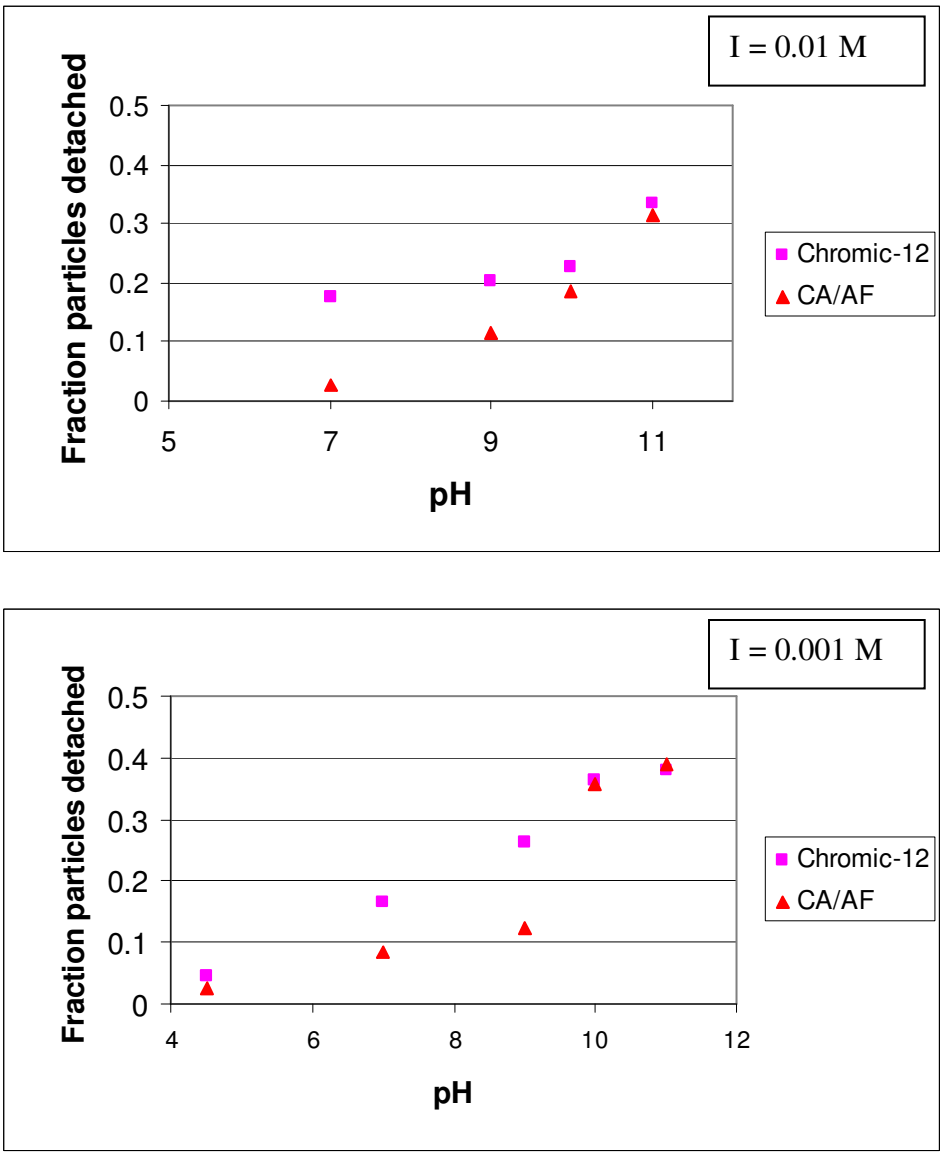

Figure 19: Fraction of colloid detachment as a function of pH and ionic strength for particles with a diameter of 1100 nm

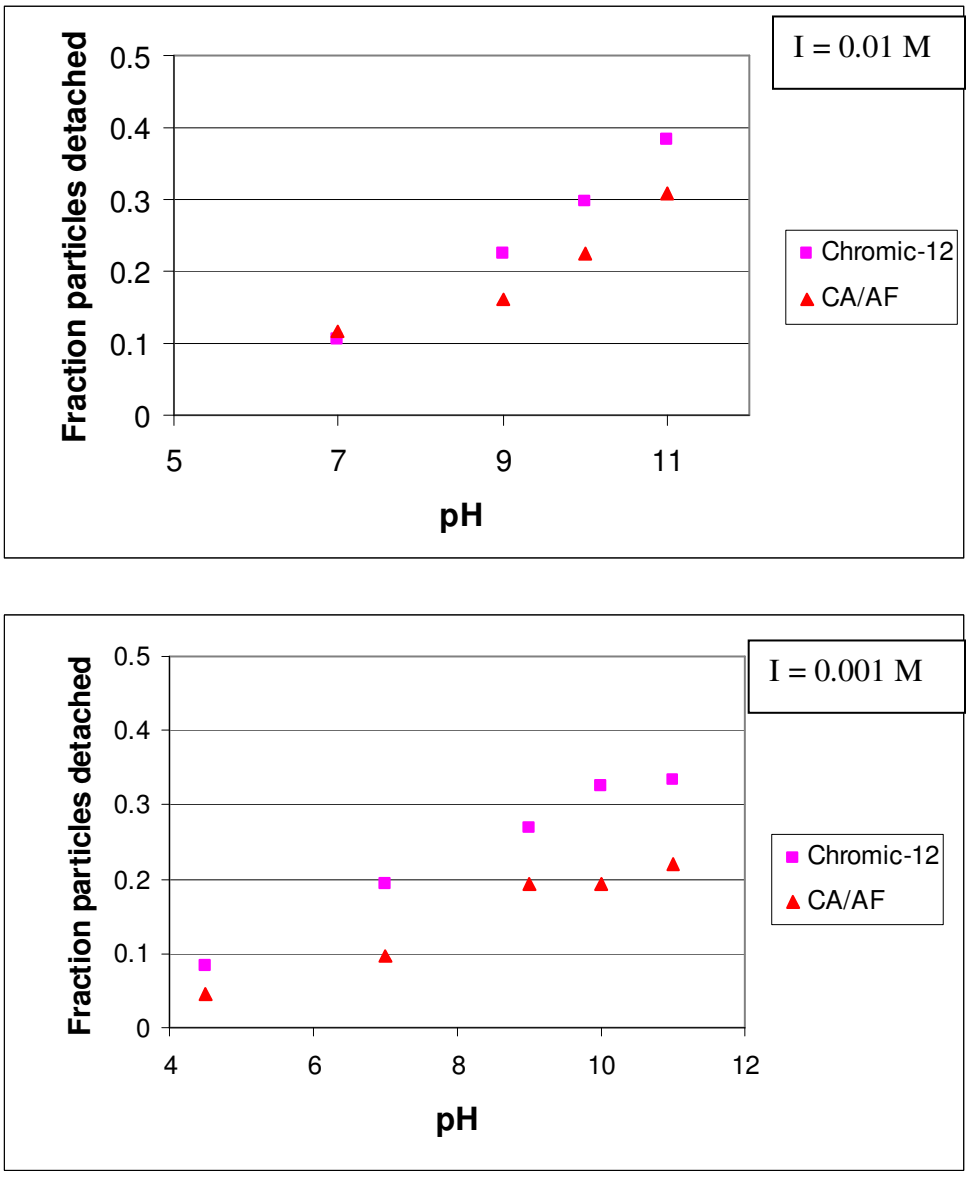

Figure 20: Fraction of colloid detachment as a function of pH and ionic strength for particles with a diameter of 510 nm

SUMMARY

Research has been done looking at the attachment and detachment of particles from porous media. Column tests with smooth glass beads have been used by other researchers to determine the effects of solution chemistry and hydrodynamic shear on detachment. However, real surfaces in the environment are not smooth. The objectives of this research were to alter and quantify the roughness of porous media, to determine its effect on colloid detachment, and develop a model to predict the effects of surface roughness on detachment.

Two batches of glass beads were chemically etched. Using a modified procedure from Logan and Shellenberger (2002), the first batch was chemically roughened using chromic acid. The second batch was chemically etched using a citric acid/ammonium fluoride solution based on a procedure used by Itälä et al. (2001). Atomic Force Microscopy was used to measure surface roughness which was defined by three parameters. The Root Mean Square (RMS) roughness and peak to valley heights (P/V height) of the two batches could not be shown statistically to be not equal. Based on the detachment trends measured in column tests, the third roughness parameter, peak to peak distance (λ), was determined to be the controlling roughness parameter.

The effects of roughness on detachment were quantified. A moment balance on the attached particle around the downstream point of contact was used to perform a parametric study. The moment balance and parametric study were used to develop a model to predict the hydrodynamic shear required for detachment based on particle diameter, P/V height, and λ. The model showed an increase in the required shear for detachment with a decrease in particle diameter and an increase in λ and P/V height.

Experimental detachment showed trends similar to those established by the model. During hydrodynamic testing less detachment was observed from surfaces with a greater λ for particles identical in size. Similarly, for solution chemistry perturbations, less detachment was observed from surfaces with a greater λ for particles identical in size. The trends found during hydrodynamic testing were attributed to the physical positioning of the attached particle on the peaks or within the "valley" of the media surface. The trends found during solution chemistry testing were attributed to a larger van der Waals attraction force for particles attached closer to the center of the porous media.

ENGINEERING IMPLICATIONS AND FUTURE WORK

Researchers have been trying to relate the principles learned in column tests to real situations to predict colloid attachment and detachment from porous media. The problems which can occur due to colloid mobilization are extensive and the mechanisms involved must be understood. The effect of roughness on colloid detachment is a significant extension to predicting the mobilization of colloids. Research has been done predicting colloid detachment from smooth surfaces. Surfaces are not smooth in natural and engineered systems. Real surfaces have "peaks" and "valleys" which cause significant alterations in the colloid detachment mechanisms. The model was developed through the use of a moment balance around the downstream point of contact. Detachment with hydrodynamic shear based on particle size, λ, and P/V height can be predicted by the model.

Colloids have been found to be naturally present in groundwater systems. Problems can arise from the detachment and mobilization of these colloids in the subsurface. Groundwater is a primary case of fluid flow through porous media where the model developed can contribute to making better predictions of colloid detachment. The installation and use of drinking water wells and groundwater sampling wells can cause changes in the pressure gradient and flowrate of groundwater. When the flowrate of the groundwater is increased, colloids detach and increase the turbidity of the water. Turbidity reduces the quality of drinking water and the accuracy of measurements in groundwater sampling.

The health of humans and animals can be affected by colloid transport. Pathogenic bio-colloids such as viruses, bacteria, protozoa, etc. can be removed from

fluid flow in natural and engineered filtration systems. Conditions which can cause these particles to become detached and mobilized back into the water stream must be defined. River bank filtration is still in certain areas around the world. This natural filtration process relies on proper particle removal to supply clean drinking water to residents in the area. Understanding the properties of the sediment and its nanoscale roughness can contribute to predicting the change in water flow required to detach and remobilize the pathogens into the water supply.

Engineered systems such as slow sand and deep bed filters in drinking water and wastewater treatment rely on significant filtration and removal of particles. Before the filters are manufactured, Atomic Force Microscopy can be used to measure the surface roughness of the media used. Knowing the size of the particles in question, the roughness can be used to predict the hydrodynamic shear required to detach pathogens once they are attached. The flowrate through filter systems can be maintained at a rate promoting attachment and preventing detachment.

Colloid mobilization has been found to significantly increase contaminant transport in the environment, primarily in groundwater. Hydrophobic contaminants such as organic solvents and radionuclides which may otherwise be stagnant due to low solubility in water may become noticeably mobile in groundwater. The contaminants adsorb to the surface of colloids which, when mobilized, carry these contaminants over significant distances. Plutonium has been thought to be immobile in groundwater due to its low solubility and high sorption to rock surfaces. Recent research at the Nevada Test Site where hundreds of underground nuclear tests have been performed has found plutonium concentrations outside detonation cavities. The findings indicate that the

transport of plutonium has been greatly increased possibly due to the detachment and mobilization of colloids in the subsurface (Kersting et al., 1999).

Colloid mobilization may not have only negative impacts on the environment. A process known as Selective Colloid Mobilization (SCM) may increase the remediation of contaminated sediment and groundwater systems. In a normal pump and treat process, contaminated groundwater can be pumped from the subsurface, treated, and then returned to the aquifer. However, in the case where a contaminant is adsorbed to colloids which are attached to the immobile solids phase, the remediation process is limited. After the water is treated and returned to the aquifer, the contaminant adsorbed to attached colloids can re-saturate the groundwater. In the SCM process, chemicals are added to the water to detach the contaminated colloids from the immobile sediment. The water containing these contaminant covered colloids is pumped to ground level, treated, and returned to the aquifer. SCM can significantly increase the remediation of groundwater contaminated with hydrophobic materials (Seaman and Bertsch, 1998).

Future column tests to obtain additional detachment data for varying roughness should be done to compare with the model developed by this research. The accuracy of accounting for the fraction of exposed area requires more investigation. The developed model is simplistic. It may be accurate when the fraction of exposed area is close to 1.0, but its accuracy may decrease when the fraction of exposed area is reduced. A computational fluid dynamics study must be done to better understand the fluid interactions with the colloid when it's attached within the "valley" of the media surface. Relating column test detachment curves to real environmental and engineered systems is the ultimate goal of research in this field. Due to the complexities and differences

between each situation, making predictions has been difficult. Continued research on the effects of roughness on detachment will significantly contribute to understanding the mechanisms responsible for colloid mobilization.

LITERATURE CITED

Amirtharajah, A., Raveendran, P. (1993). *Colloids and Surfaces. A: Physiochemical and Engineering Aspects, 73*, 211.

Bai, R., Tien, C. (1997). Particle Detachment in Deep Bed Filtration. *Journal of Colloid and Interface Science, 186*, 307-317.

Beach, E.R., Tormoen, G.W., Drelich, J., Han, R. (2001). Pull-off Force Measurements Between Rough Surfaces by Atomic Force Microscopy. *Journal of Colloid and Interface Science, 247*, 84-99.

Bergendahl, J., Grasso, D. (1998). Colloid generation during batch leaching tests: Mechanics of disaggregation. *Colloids and Surfaces. A: Physiochemical and Engineering Aspects, 135*, 193-205.

Bergendahl, J., Grasso, D. (1999). Prediction of Colloid Detachment in a Model Porous Media: Thermodynamics. *AIChE Journal, 45*, 475-484.

Bergendahl, J., Grasso, D. (2000). Prediction of Colloid Detachment in a Model Porous Media: Hydrodynamics. *Chemical Engineering Science 55*, 1523-1532.

Derjaguin, B.V., Landau, L.D. (1941). Theory of the Stability of Strongly Charged Lyophobic Sols and of the Adhesion of Strongly Charged Particles in Solutions of Electrolytes. *Acta Physicochim. URSS, 14*, 733-762.

Elimelech, M. (1994). Particle Deposition on Ideal Collectors from Dilute Flowing Suspensions: Mathematical Formulation, Numerical Solution, and Simulations. *Separation Technology, 4*, 186-212.

Elimelech, M., Gregory, J., Jia, X., Williams, R. (1995). *Particle Deposition and Aggregation,* 1st ed., Butterworth-Heinmann, Oxford, pp. 36, 50.

Freitas, A.M., Sharma, M.M. (1999). Effect of Surface Hydrophobicity on the Hydrodynamic Detachment of Particles from Surfaces. *Langmuir, 15*, 2466-2476.

Gregory, J. (1975). Interaction of Unequal Double Layers at Constant Charge. *Journal of Colloid and Interface Science, 51*, 44.

Gregory, J. (1981). Approximate Expressions for Retarded van der Waals Interaction. *Journal of Colloid and Interface Science, 83*, 138.

Israelachvili, J.N. (1992). In *Intermolecular and Surface Forces*, 2nd ed., Academic Press, London.

Itälä, A., Nordström, E.G., Ylänen, H., Aro, H.T., Hupa, M. (2001). Creation of Microrough Surface on Sintered Bioactive Glass Microspheres. *Journal of Biomedical Materials Research, 56*, 282-288.

Johnson, K.L., Kendall, K., Roberts, A.D. (1971). *Procedures of the Royal Society. London. A., 324*, 301.

Kallay, N., Barouch, E., Matijević, E. (1987). Diffusional Detachment of Colloidal Particles from Sold/Solution Interfaces. *Advances in Colloid and Interface Science, 27*, 1-42.

Kersting, A.B., Efurd, D.W., Finnegan, D.L., Rokop, D.J., Smith, D.K., Thompson, J.L. (1999). Migration of Plutonium in Ground Water at the Nevada Test Site. *Nature, 397*, 56-59.

Litton, G.M., Olsen, T.M. (1993). *Environmental Science & Technology, 27*, 185-193.

Liu, D., Johnson, P.R., Elimelech, M. (1995). Colloid Deposition Dynamics in Flow Through Porous Media: Role of Electrolyte Concentration. *Environmental Science and Technology, 29*, 2963-2973.

Mays, L.W. (2001). *Water Resources Engineering*, John Wiley & Sons, Inc., New York.

Rabinovich, Y.I., Adler, J.J., Ata, A., Singh, R.K., Moudgil, B.M. (2000). Adhesion Between Nanoscale Rough Surfaces. *Journal of Colloid and Interface Science 232*, 17-24.

Rijnaarts, H.M., Norde, W., Bouwer, E.J., Lyklema, J. Zehnder, A.J.B. (1996). Bacterial Deposition in Porous Media Related to the Clean Bed Collision Efficiency and to Substratum Blocking by Attached Cells. *Environmental Science and Technology, 30*, 2869-2876.

Ruckenstein, E., Prieve, D.C. (1976). Adsorption and Desorption of Particles and Their Chromatographic Separation. *AIChE Journal, 22*, 276.

Ryan, J.N., Elimelech, M. (1996). Colloid Mobilization and Transport in Groundwater. *Colloids and Surfaces. A: Physiochemical and Engineering Aspects, 107*, 1-56.

Ryan, J.N., Gschwend, P.M. (1994). Effects of Ionic Strength and Flow Rate on Colloid Release: Relating Kinetics to Intersurface Potential Energy. *Journal of Colloid and Interface Science, 164*, 21-34.

Ryde, N.P., Matijević, E. (2000). Deposition and Detachment Studies of Fine Particles by the Packed Column Technique. *Colloids and Surfaces. A: Physiochemical and Engineering Aspects, 165*, 59-78.

Seaman, J.C., Bertsch, P.M. (1998). Enhancing Aquifer Reclamation through Selective Colloid Mobilization. *EPA Ground Water Currents, 29*.

Shellenberger, K., Logan, B.E. (2002). Effect of Molecular Scale Roughness of Glass Beads on Colloidal and Bacterial Deposition. *Environmental Science & Tecnology, 36*, 184-189.

Tobiason, J.E. (1989). Chemical Effects on the Deposition of Non-Brownian Particles. *Colloids Surfaces, 39*, 53-77.

van Oss, C.J. (1994) *Interfacial Forces in Aqueous Media,* 1st ed., Marcel Dekker, New York.

Verwey, E.J.W., Overbeek, J.Th.G. (1948). *Theory of the Stability of Lyophobic Colloids,* Elsevier, Amsterdam.

APPENDIX A: CONCENTRATION-OPTICAL DENSITY RELATIONSHIPS

Latex particles with a diameter of 1100 nm, OD measured with λ = 650 nm

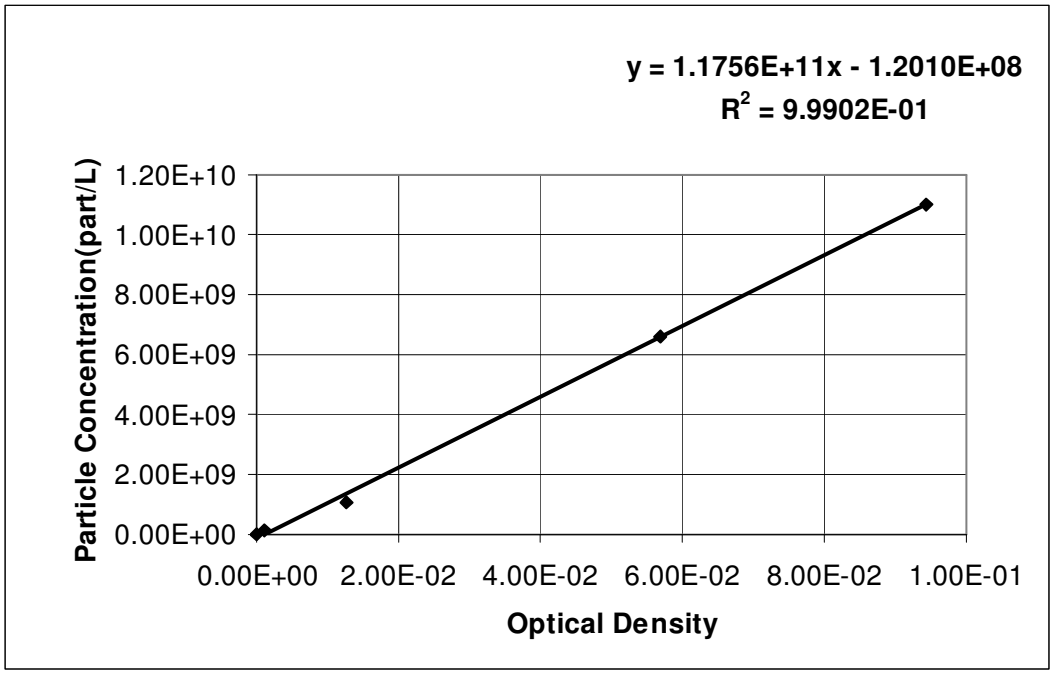

Latex particles with a diameter of 510 nm, OD measured with λ = 650 nm

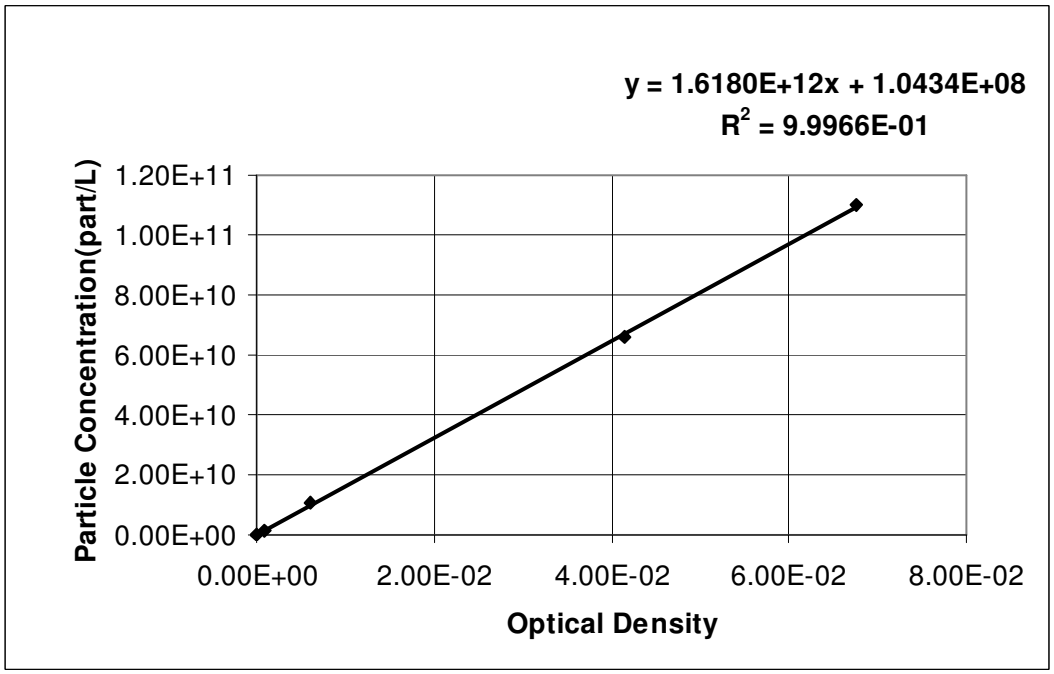

Latex particles with a diameter of 120 nm, OD measured with λ = 500 nm

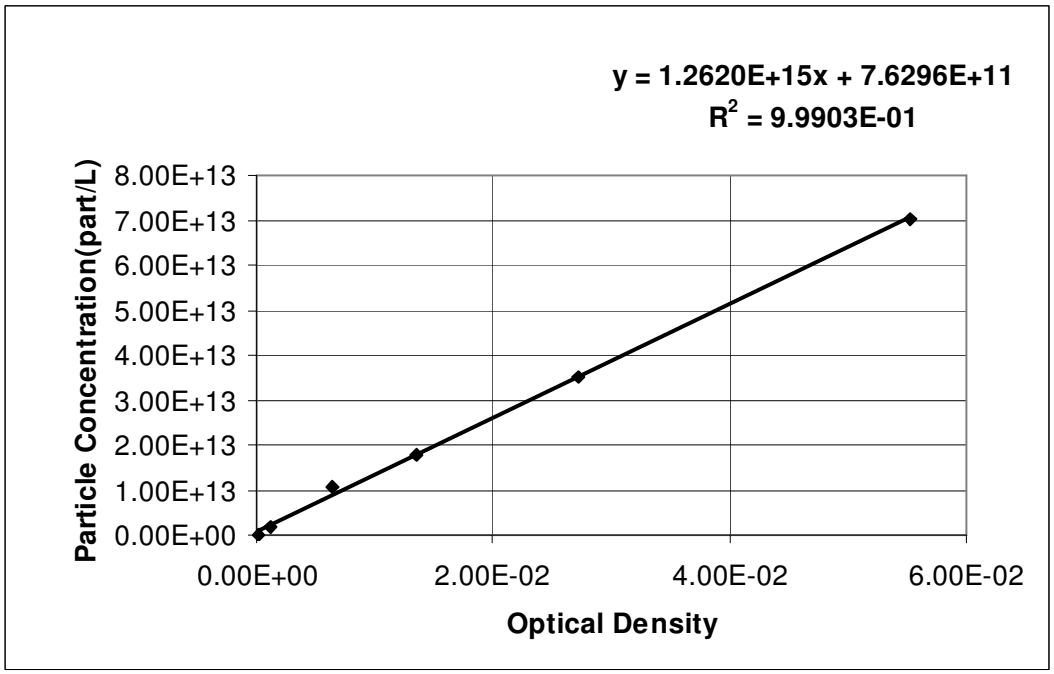

APPENDIX B: MEDIA SURFACE ROUGHNESS PARAMETERS

Peak to Peak Distances (λ-values)

Lambda 1 Values for Section 0-5000 nm

Bead/Area	Chromic 12	CA/AF
-	λ1 (nm)	λ1 (nm)
B1/A1-35	1240.15748	2303.14961
B1/A1-201	1082.67717	1771.65354
B1/A1-400	944.88189	1574.80315
B1/A2-35	925.19685	1259.84252
B1/A2-201	679.34783	1259.84252
B1/A2-400	649.60630	1181.10236
B1/A3-35	629.92126	1122.04724
B1/A3-201	629.92126	1023.62205
B1/A3-400	590.55118	984.25197
B2/A1-35	570.86614	748.03150
B2/A1-201	551.18110	708.66142
B2/A1-400	516.30435	688.97638
B2/A2-35	516.30435	649.60630
B2/A2-201	511.81102	649.60630
B2/A2-400	489.13043	649.60630
B2/A3-35	461.95652	649.60630
B2/A3-201	452.75591	590.55118
B2/A3-400	452.75591	570.86614
B3/A1-35	413.38583	531.49606
B3/A1-201	407.60870	531.49606
B3/A1-400	407.60870	511.81102
B3/A2-35	374.01575	413.38583
B3/A2-201	314.96063	413.38583
B3/A2-400	298.91304	374.01575
B3/A3-35	275.59055	374.01575
B3/A3-201	255.90551	354.33071
B3/A3-400	236.22047	334.64567
Mean	**551.09393**	**823.12628**
Stan.Dev.	**248.15192**	**482.77108**
95%C.I.	**93.60172**	**182.09896**
95%C.I. Range	**97.50%**	**2.50%**
Chromic-12	**644.69565**	**457.49221**
CA/AF	**1005.22523**	**641.02732**

Lambda 2 Values for Section 2000-2500 nm

Bead/Area	Chromic 12	CA/AF
-	λ2 (nm)	λ2 (nm)
B1/A1-35	100.39370	96.45669
B1/A1-201	96.45669	94.48819
B1/A1-400	88.58268	72.83465
B1/A2-35	88.58268	70.86614
B1/A2-201	76.77165	66.92913
B1/A2-400	74.80315	66.92913
B1/A3-35	68.89764	64.96063
B1/A3-201	68.89764	62.99213
B1/A3-400	62.99213	62.99213
B2/A1-35	59.05512	59.05512
B2/A1-201	57.08661	53.14961
B2/A1-400	57.08661	51.18110
B2/A2-35	55.11811	49.21260
B2/A2-201	55.11811	47.24409
B2/A2-400	51.18110	47.24409
B2/A3-35	51.18110	47.24409
B2/A3-201	51.18110	45.27559
B2/A3-400	47.24409	45.27559
B3/A1-35	47.24409	43.30709
B3/A1-201	43.30709	41.33858
B3/A1-400	41.33858	41.33858
B3/A2-35	39.37008	39.37008
B3/A2-201	37.40157	39.37008
B3/A2-400	35.43307	39.37008
B3/A3-35	35.43307	35.43307
B3/A3-201	31.49606	35.43307
B3/A3-400	31.49606	35.43307
Mean	**57.52406**	**53.87868**
Stan.Dev.	**19.72538**	**16.58824**
95%C.I.	**7.44032**	**6.25701**
95%C.I. Range	**97.50%**	**2.50%**
Chromic-12	**64.96438**	**50.08374**
CA/AF	**60.13569**	**47.62168**

Mean λ_1 Values with Bars representing 95% Confidence Intervals

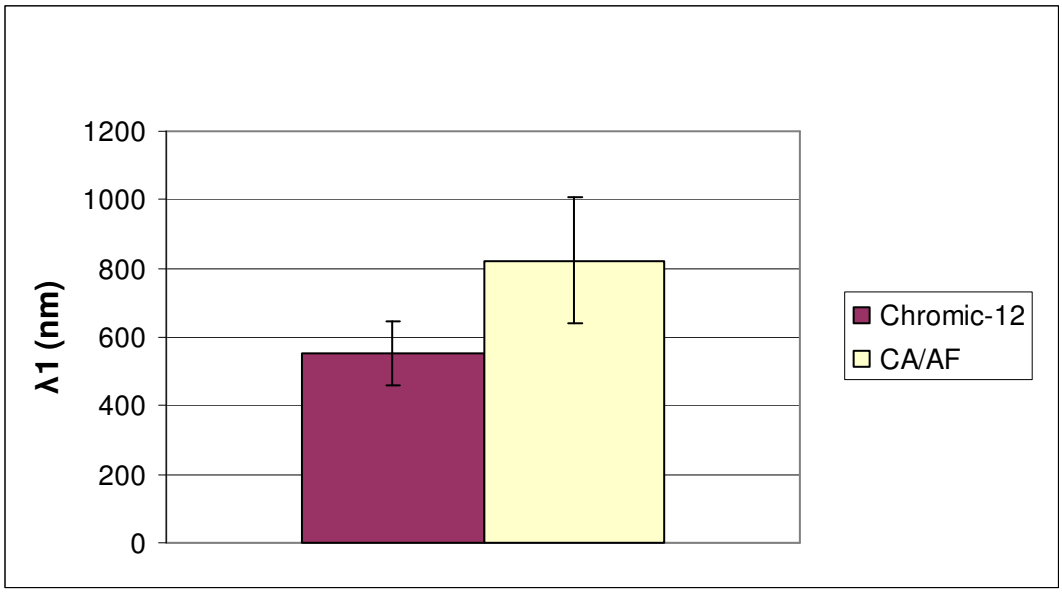

Mean λ_2 Values with Bars representing 95% Confidence Intervals

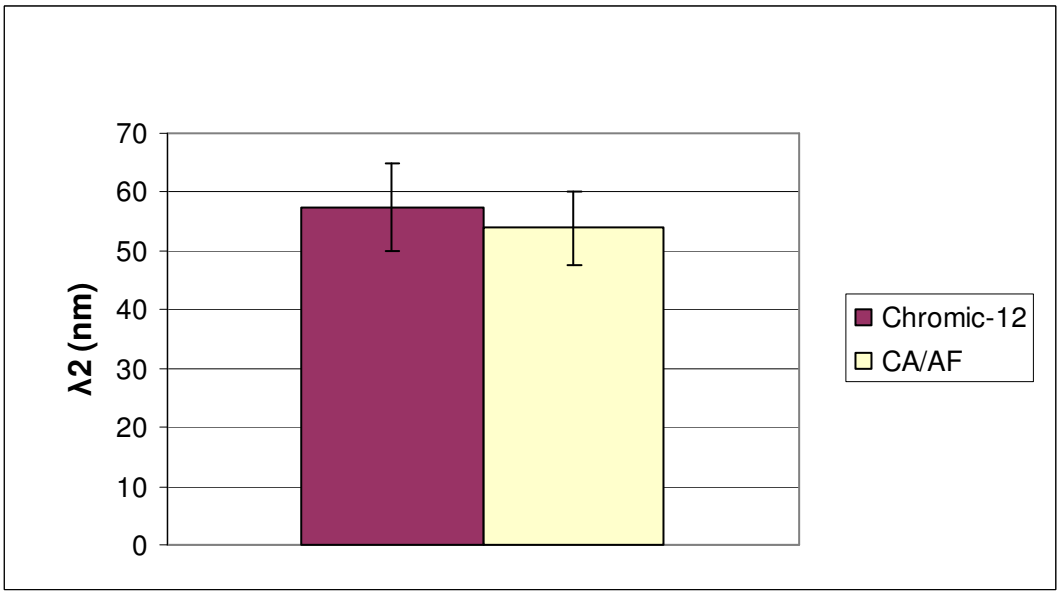

Peak to Valley Heights (P/V Heights)

P/V Height 1 for Section 0-5000 nm

Bead/Area	Chromic-12	CA/AF
-	P/V Height (nm)	P/V Height (nm)
B1/A1-35	1752.80899	1000.00000
B1/A1-201	1132.58427	802.24719
B1/A1-400	1904.49438	261.23596
B1/A2-35	1069.66292	808.98876
B1/A2-201	778.65169	640.44944
B1/A2-400	651.68539	313.48315
B1/A3-35	422.47191	1264.04494
B1/A3-201	393.25843	1924.15730
B1/A3-400	795.50562	950.56180
B2/A1-35	485.39326	438.20225
B2/A1-201	499.43820	365.16854
B2/A1-400	453.93258	588.76404
B2/A2-35	1594.38202	1159.55056
B2/A2-201	1460.67416	795.50562
B2/A2-400	950.56180	407.86517
B2/A3-35	1966.29213	1418.53933
B2/A3-201	660.67416	2123.59551
B2/A3-400	1365.16854	835.95506
B3/A1-35	925.84270	1078.65169
B3/A1-201	333.70787	1137.64045
B3/A1-400	468.53933	896.62921
B3/A2-35	606.74157	825.84270
B3/A2-201	2292.13483	788.76404
B3/A2-400	617.97753	559.55056
B3/A3-35	752.80899	1456.17978
B3/A3-201	523.03371	1617.97753
B3/A3-400	808.98876	534.83146
Mean	**950.64503**	**925.71785**
Stan.Dev.	**549.34321**	**475.57778**
95%C.I.	**207.20965**	**179.38568**

95%C.I. Range	97.50%	2.50%
Chromic-12	1157.85467	743.43538
CA/AF	1105.10353	746.33218

P/V Height 2 for Section 2000-2500 nm

Bead/Area	Chromic-12	CA/AF
-	P/V Height (nm)	P/V Height (nm)
B1/A1-35	134.07821	61.45251
B1/A1-201	125.13966	37.98883
B1/A1-400	184.35754	22.34637
B1/A2-35	80.44693	70.39106
B1/A2-201	109.49721	22.34637
B1/A2-400	72.62570	154.18994
B1/A3-35	58.10056	418.99441
B1/A3-201	27.37430	159.77654
B1/A3-400	46.92737	321.78771
B2/A1-35	110.61453	90.50279
B2/A1-201	129.05028	58.65922
B2/A1-400	125.13966	111.73184
B2/A2-35	147.48603	122.90503
B2/A2-201	223.46369	67.03911
B2/A2-400	221.22905	38.54749
B2/A3-35	312.84916	237.43017
B2/A3-201	195.53073	218.99441
B2/A3-400	221.22905	125.13966
B3/A1-35	71.50838	80.44693
B3/A1-201	53.63128	117.31844
B3/A1-400	63.68715	140.78212
B3/A2-35	44.69274	89.38547
B3/A2-201	39.10615	127.37430
B3/A2-400	312.84916	120.67039
B3/A3-35	50.27933	170.94972
B3/A3-201	50.83799	117.31844
B3/A3-400	50.27933	89.38547
Mean	**120.81523**	**125.69832**
Stan.Dev.	**82.01871**	**89.43810**
95%C.I.	**30.93707**	**33.73563**

95%C.I. Range	97.50%	2.50%
Chromic-12	151.75229	89.87816
CA/AF	159.43395	91.96270

Mean $(P/V)_1$ Height Values with Bars representing 95% Confidence Intervals

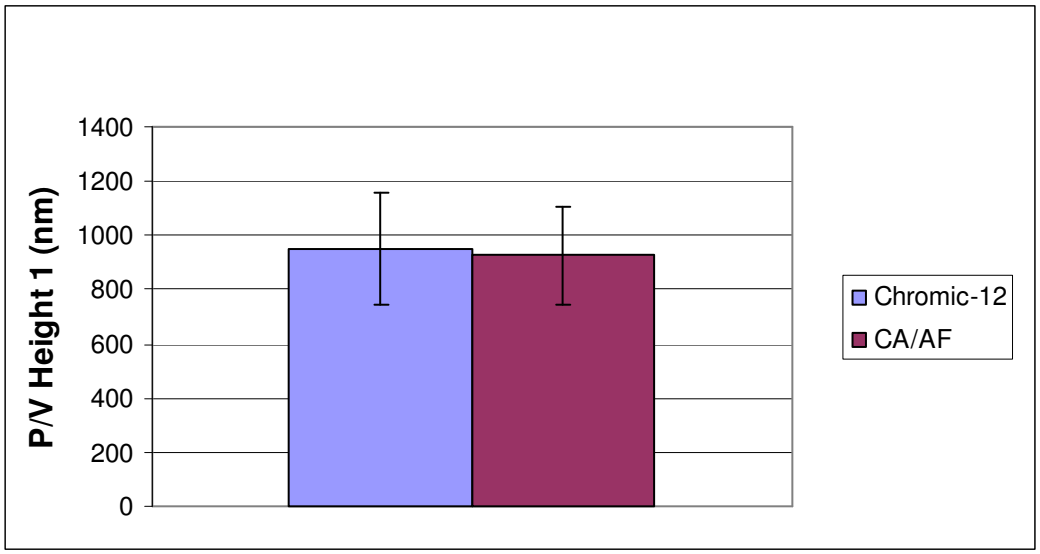

Mean $(P/V)_2$ Height Values with Bars representing 95% Confidence Intervals

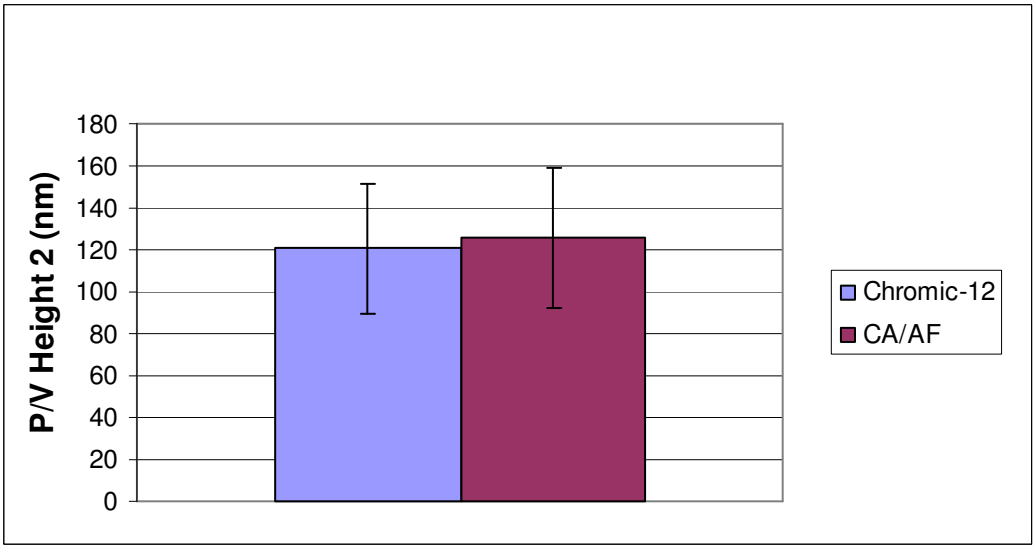

Root Mean Square Roughness Values (RMS Values)

RMS 1 for Bead Area of 5.0 um x 5.0 um

Bead/Area -	CA/AF RMS1 (nm)	Chromic 12 RMS1 (nm)
B1/A1	476.80431	352.69941
B1/A2	449.47571	295.07776
B1/A3	309.49647	261.98168
B2/A1	271.34148	226.01961
B2/A2	252.34891	209.73206
B2/A3	237.62771	197.06271
B3/A1	233.43891	169.94147
B3/A2	200.51909	166.99659
B3/A3	100.83686	104.26560
Average	**281.32105**	**220.41965**
Stan.Dev.	**118.07192**	**74.48501**
95%C.I.	**77.13891**	**48.66265**
95%C.I. Range	**97.50%**	**2.50%**
CA/AF	**358.45996**	**204.18214**
Chromic-12	**269.08230**	**171.75701**

RMS 2 for Bead Area of 250 nm x 250 nm

Bead/Area -	CA/AF RMS2 (nm)	Chromic 12 RMS2 (nm)
B1/A1-A	378.92436	580.82046
B1/A1-B	307.60129	471.26572
B1/A1-C	274.31957	330.13239
B1/A2-A	230.55546	206.83883
B1/A2-B	220.20407	198.82574
B1/A2-C	212.91467	181.59376
B1/A3-A	157.31444	163.07705
B1/A3-B	154.68621	157.77777
B1/A3-C	139.48322	146.90503
B2/A1-A	137.11903	144.51637
B2/A1-B	132.34478	140.81311
B2/A1-C	131.50706	133.41427
B2/A2-A	128.36989	117.74548
B2/A2-B	116.91335	116.56458
B2/A2-C	111.89691	113.77761
B2/A3-A	102.43193	99.31435
B2/A3-B	95.82859	98.64025
B2/A3-C	90.92263	90.45005
B3/A1-A	89.28720	83.36587
B3/A1-B	85.48321	81.40372
B3/A1-C	81.50851	76.19531
B3/A2-A	73.16047	69.36725
B3/A2-B	69.52019	59.48656
B3/A2-C	65.75190	59.14541
B3/A3-A	63.79285	49.91715
B3/A3-B	54.20932	41.63193
B3/A3-C	48.47181	40.46473
Average	**139.05640**	**150.12780**
Stan.Dev.	**82.38838**	**125.88636**
95%C.I.	**31.07650**	**47.48373**
95%C.I. Range	**97.50%**	**2.50%**
CA/AF	**170.13291**	**107.97990**
Chromic-12	**197.61154**	**102.64407**

Mean RMS_1 Values with Bars representing 95% Confidence Intervals

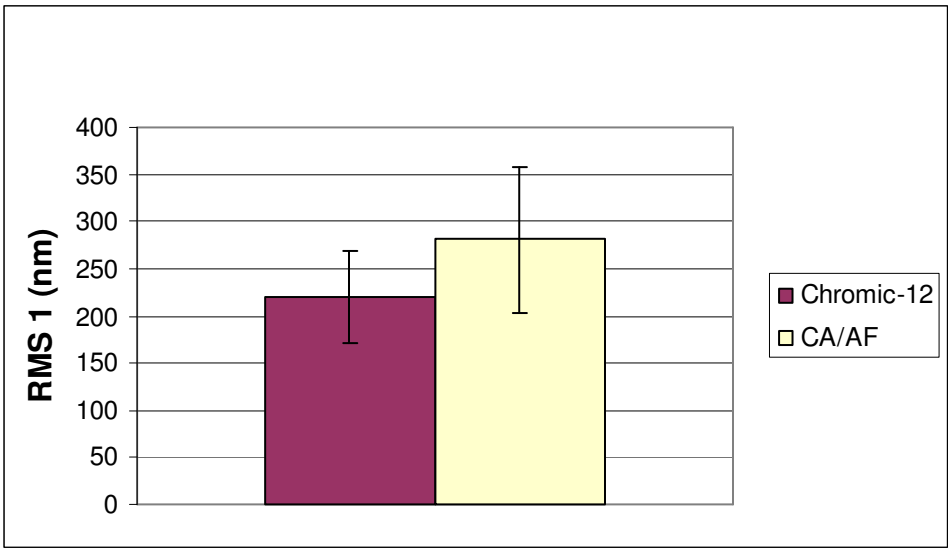

Mean RMS_1 Values with Bars representing 95% Confidence Intervals

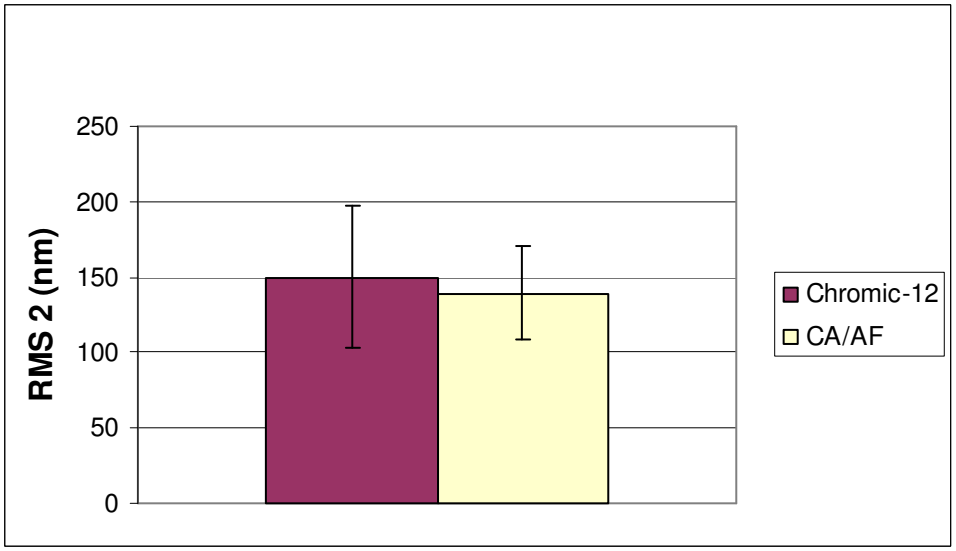

APPENDIX C: DATA FOR EXPERIMENTAL DETACHMENT WITH HYDRODYNAMIC SHEAR CHANGES

Particles with a Diameter of 1100 nm

M4Z	Chromic-12	CA/AF
Flowrate (mL/min)	Cumulative Fraction Detachment	Cumulative Fraction Detachment
5	0	0
25	0.019427511	0.003028958
50	0.027561872	0.014790268
75	0.460044448	0.341353011
100	0.619448345	0.448178559

M5Z	Chromic-12	CA/AF
Flowrate (mL/min)	Cumulative Fraction Detachment	Cumulative Fraction Detachment
5	0	0
25	0.041725218	0.000489954
50	0.161658722	0.002630475
75	0.557830529	0.266395618
100	0.614392044	0.479812718

M6Z	Chromic-12	CA/AF
Flowrate (mL/min)	Cumulative Fraction Detachment	Cumulative Fraction Detachment
5	0	0
25	0.036684308	0.004202792
50	0.07968887	0.017201712
75	0.582351358	0.300657569
100	0.610800481	0.420707791

M7Z	Chromic-12	CA/AF
Flowrate (mL/min)	Cumulative Fraction Detachment	Cumulative Fraction Detachment
5	0	0
25	0.005170574	0.000973878
50	0.074939058	0.016569577
75	0.574725122	0.292173796
100	0.601682113	0.411383003

Particles with a Diameter of 510 nm

M4Z	Chromic-12	CA/AF
Flowrate (mL/min)	Cumulative Fraction Detachment	Cumulative Fraction Detachment
5	0	0
25	0.010393756	0.001654919
50	0.040267944	0.011150274
75	0.42499461	0.352771724
100	0.464824505	0.403493149

M5Z	Chromic-12	CA/AF
Flowrate (mL/min)	Cumulative Fraction Detachment	Cumulative Fraction Detachment
5	0	0
25	0.004396924	0.000443973
50	0.017265307	0.003767551
75	0.371777149	0.273512861
100	0.411597824	0.33246622

M6Z	Chromic-12	CA/AF
Flowrate (mL/min)	Cumulative Fraction Detachment	Cumulative Fraction Detachment
5	0	0
25	0.010454429	0.000892655
50	0.051514669	0.006393409
75	0.359251273	0.353133177
100	0.372388872	0.394070392

M6Z	Chromic-12	CA/AF
Flowrate (mL/min)	Cumulative Fraction Detachment	Cumulative Fraction Detachment
5	0	0
25	0.000910559	0.000745585
50	0.03780414	0.034899105
75	0.461876583	0.302565064
100	0.475061049	0.33668997

Particles with a Diameter of 120 nm

M4Z	Chromic-12	CA/AF
Flowrate (mL/min)	Cumulative Fraction Detachment	Cumulative Fraction Detachment
5	0	0
25	0.071118859	0.024586445
50	0.089676976	0.040988317
75	0.17691128	0.259965834
100	0.224621226	0.315377296

M5Z	Chromic-12	CA/AF
Flowrate (mL/min)	Cumulative Fraction Detachment	Cumulative Fraction Detachment
5	0	0
25	0.026232188	0.068035559
50	0.045201356	0.092840503
75	0.128729427	0.262853859
100	0.19624299	0.316311789

M6Z	Chromic-12	CA/AF
Flowrate (mL/min)	Cumulative Fraction Detachment	Cumulative Fraction Detachment
5	0	0
25	0.03631388	0.017321566
50	0.054352963	0.031568518
75	0.146379775	0.197387251
100	0.206288137	0.238247856

M7Z	Chromic-12	CA/AF
Flowrate (mL/min)	Cumulative Fraction Detachment	Cumulative Fraction Detachment
5	0	0
25	0.054790746	0.019016945
50	0.07384787	0.041411816
75	0.165544169	0.211238459
100	0.208921011	0.27389431

APPENDIX D: DATA FOR EXPERIMENTAL DETACHMENT WITH SOLUTION CHEMISTRY CHANGES

Particles with a Diameter of 1100 nm

M1	Chromic-12	CA/AF
pH	Cumulative Fraction	Cumulative Fraction
-	Detachment	Detachment
7	0.176518106	0.026668073
9	0.203421982	0.115776681
10	0.227717232	0.187346537
11	0.333018566	0.315632624

M2	Chromic-12	CA/AF
pH	Cumulative Fraction	Cumulative Fraction
-	Detachment	Detachment
4.5	0.045505634	0.025444119
7	0.164892691	0.085153189
9	0.261379705	0.123654097
10	0.36279998	0.358642866
11	0.379029032	0.390151672

Particles with a Diameter of 510 nm

M1	Chromic-12	CA/AF
pH	Cumulative Fraction	Cumulative Fraction
-	Detachment	Detachment
7	0.106313384	0.1160905
9	0.226275591	0.161125623
10	0.297441581	0.224438022
11	0.384083477	0.308558241

M2	Chromic-12	CA/AF
pH	Cumulative Fraction	Cumulative Fraction
-	Detachment	Detachment
4.5	0.084640697	0.045738366
7	0.192380249	0.096768632
9	0.269098561	0.192387715
10	0.326344857	0.192976492
11	0.334133564	0.220932812

Particles with a Diameter of 120 nm

M1	Chromic-12	CA/AF
pH	Cumulative Fraction	Cumulative Fraction
-	Detachment	Detachment
7	0.006964273	0.016578382
9	0.039962899	0.030446348
10	0.043662163	0.054821137
11	0.075818169	0.080949167

M2	Chromic-12	CA/AF
pH	Cumulative Fraction	Cumulative Fraction
-	Detachment	Detachment
4.5	0.038098853	0.006750271
7	0.070491913	0.032517269
9	0.095290284	0.068572698
10	0.122725943	0.13875943
11	0.129000682	0.172732443

APPENDIX E: NORMALIZED DETACHMENT DATA AT A FLOWRATE OF 75 mL/min FOR FLOWRATE PERTURBATION EXPERIMENTS

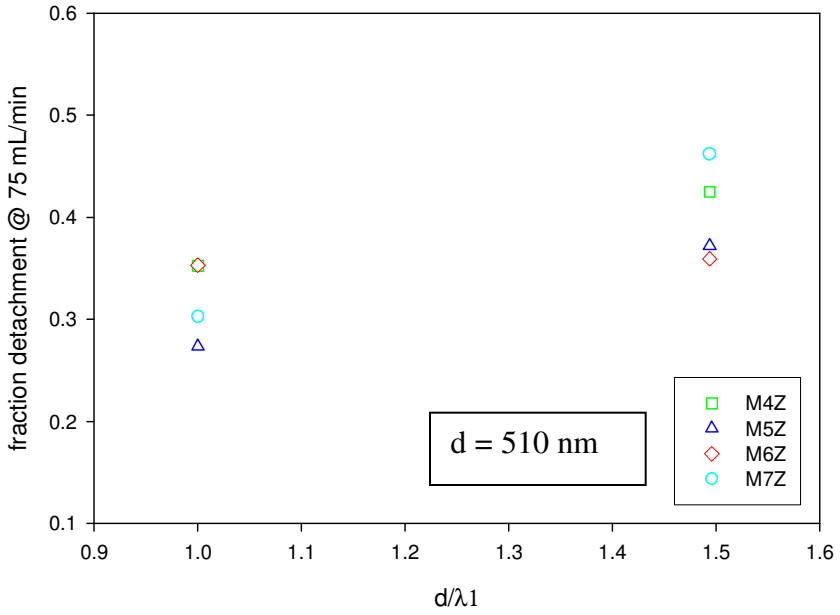
fraction detachment @ 75 mL/min
0.6
0.5
0.4
0.3
0.2
0.1
0.9
1.0
1.1
1.2
1.3
1.4
1.5
1.6
d/λ1
d = 510 nm
M4Z
M5Z
M6Z
M7Z

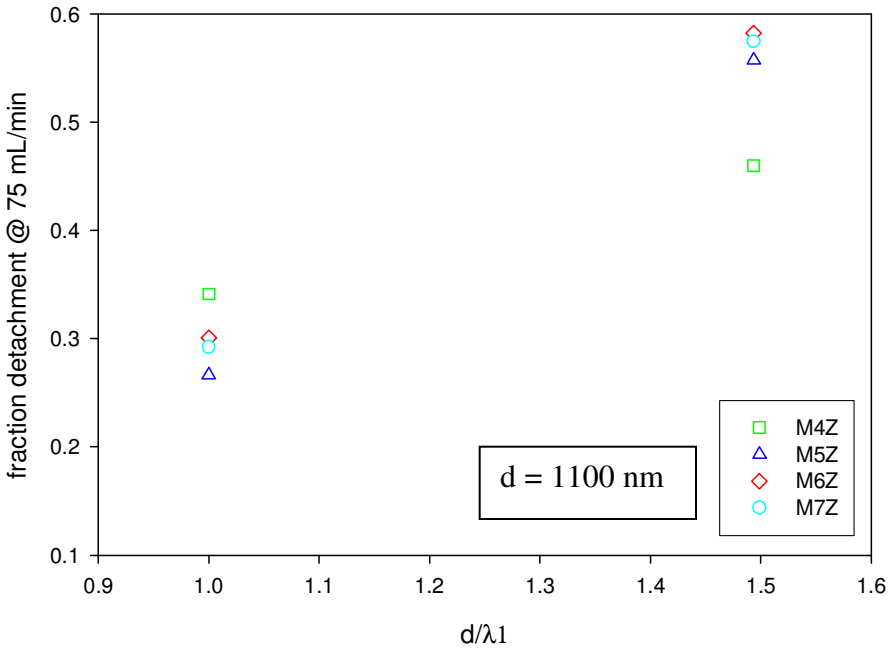
fraction detachment @ 75 mL/min
0.6
0.5
0.4
0.3
0.2
0.1
0.9
1.0
1.1
1.2
1.3
1.4
1.5
1.6
d/λ1
d = 1100 nm
M4Z
M5Z
M6Z
M7Z

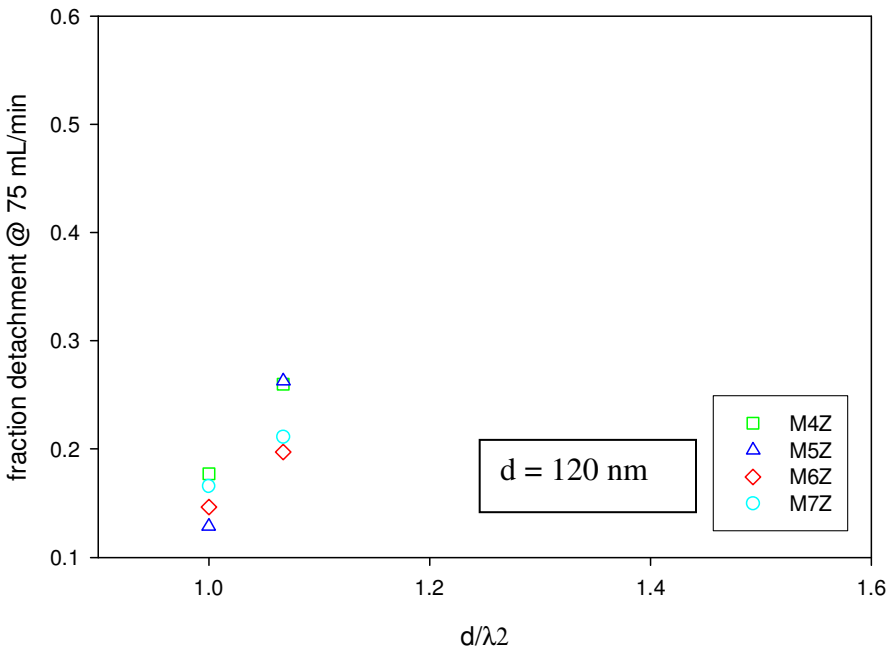
0.6
0.5
0.4
0.3
0.2
0.1
fraction detachment @ 75 mL/min
1.0
1.2
1.4
1.6
d/λ2
d = 120 nm
M4Z
M5Z
M6Z
M7Z

APPENDIX F: MATHCAD SHEETS FOR MOMENT BALANCE ANALYSIS ON ATTACHED COLLOIDS

To Determine X and Z Values when Y = P/V Height (Colloid Attachment to Peaks)

(m = nm)

$\lambda := 400m$ $R := 250m$

Initial Guesses

$X := 200m$ $Z := 200m$

Given

$X = \frac{\lambda}{2}$ $X^2 + Z^2 = R^2$

$\text{Find}(X, Z) = \begin{pmatrix} 200 \\ 150 \end{pmatrix} m$

To Determine X and Z Values when Y < P/V Height (Colloid Attached in Valley)

(m = nm)

$\lambda := 400\text{m}$ $\quad H := 1000\text{m}$ $\quad \dfrac{\left(\frac{\lambda}{2}\right)}{H} = 0.2$

$\theta := \operatorname{atan}\left[\dfrac{\left(\frac{\lambda}{2}\right)}{H}\right]$ $\quad \theta = 0.1973955598$ $\quad r := 150\,\text{m}$

$b := \dfrac{r}{\sin(\theta)}$ $\quad b = 764.8529277\text{m}$ $\quad a := 0\text{m}$

Initial Guesses $\quad x := 25\cdot\text{m}$ $\quad y := 50\cdot\text{m}$ $\quad z := 20\text{m}$

Given

$\dfrac{x}{y} = \dfrac{\left(\frac{\lambda}{2}\right)}{H}$ $\quad (x-a)^2 + (y-b)^2 = r^2$ $\quad z = b - y$

$\text{Find}(x, y, z) = \begin{pmatrix} 147.0871018 \\ 735.4355089 \\ 29.4174181 \end{pmatrix}\text{m}$

Shear Requirement to Achieve a Detachment of 50%

$\mu := 8.998\,10^{-4}\,N\cdot\frac{s}{m^2}$ $\quad \nu := 9.025\,10^{-7}\,\frac{m^2}{s}$ $\quad Fa := 1.485\,410^{-12}\,N$

$X := 150\,10^{-9}\,m$ $\quad Z := 529.151\,0^{-9}\,m$ $\quad R := 550\,10^{-9}\,m$

$S := \mathbf{48.325}\cdot\frac{1}{s}$ $\quad A := 0.995($

$Fd := 10.205A\cdot\pi\cdot\mu\cdot S\cdot R^2$

$Fd = 4.198\times 10^{-13}\,N$

$Fl := 81.2\mu\cdot R^3\cdot\frac{S^{\left(\frac{3}{2}\right)}}{\nu^{\left(\frac{1}{2}\right)}}$

$Fl = 4.299\times 10^{-15}\,N$

$Fa = 1.4854\times 10^{-12}\,N$

$\frac{(Fd\cdot Z + Fl\cdot X)}{X} = 1.4854\times 10^{-12}\,N$

APPENDIX G: PARAMETRIC STUDY

Parametric Study
(P/V Height = 1000 nm)

λ (nm)	Part. Diam. (nm)	P-V Height (nm)	X (nm)	Z (nm)	Fraction Exp.Area	Shear (s-1)
300	1300	1000	150	632.4560	0.9973	34.17
400	1300	1000	200	618.4660	0.9936	46.698
500.01	1300	1000	250.005	599.9980	0.9873	60.445
600	1300	1000	300	576.6280	0.9776	76.04
700	1300	1000	350	547.7230	0.9634	94.48
800	1300	1000	400	512.3480	0.9434	117.37
900	1300	1000	450	469.0420	0.9156	147.67
1000.01	1300	1000	500.005	415.3250	0.8771	191.4
1100	1300	1000	550	346.4100	0.8225	263.71
1200	1300	1000	557.3704	334.4223	0.7507	299.81
1300	1300	1000	544.9976	354.2282	0.6859	302.62
300	1100	1000	150	529.1500	0.9956	48.326
400	1100	1000	200	512.3480	0.9894	66.844
500.01	1100	1000	250.005	489.895	0.9787	88.125
600	1100	1000	300	460.977	0.9619	113.96
700	1100	1000	350	424.264	0.9367	147.6
800	1100	1000	400	377.492	0.8997	195.75
900	1100	1000	450	316.228	0.8447	275.46
1000.01	1100	1000	491.934	245.9695	0.7581	416.22
1100	1100	1000	481.9187	265.0553	0.6617	431.6
1200	1100	1000	471.6211	282.9727	0.5797	449.25
1300	1100	1000	461.144	299.7436	0.5106	468.12
300	900	1000	150	424.264	0.9919	73.88
400	900	1000	200	403.113	0.9801	104.66
500.01	900	1000	250.005	374.162	0.9595	143.44
600	900	1000	300	335.41	0.9259	197.74
700	900	1000	350	282.843	0.8720	286.94
800	900	1000	400	206.155	0.7811	484.94
900	900	1000	410.3647	184.6641	0.6356	656.78
1000.01	900	1000	402.4914	201.2477	0.5088	725.58
300	700	1000	150	316.228	0.9823	128.51
400	700	1000	200	287.228	0.9557	193.063
500.01	700	1000	250.005	244.944	0.9059	296.018
600	700	1000	300	180.278	0.8128	524.68
700	700	1000	330.3504	115.6227	0.6077	1097.99
300	500	1000	150	200	0.9480	293.615
400	500	1000	200	150	0.8576	568.186
500.01	500	1000	242.5353	60.635	0.5781	2135.866
300	300	1000	148.3405	22.252	0.5474	5574.1

Parametric Study
(P/V Height = 500 nm)

λ (nm)	Part. Diam. (nm)	P-V Height (nm)	X (nm)	Z (nm)	Fraction Exp.Area	Shear (s^{-1})
300	1300	500	150	632.4560	0.9973	34.17
400	1300	500	200	618.4660	0.9936	46.698
500.01	1300	500	250.005	599.9980	0.9873	60.444
600	1300	500	300	576.6280	0.9776	76.04
700	1300	500	350	547.7230	0.9634	94.48
800	1300	500	400	512.3480	0.9434	117.37
900	1300	500	450	469.0420	0.9156	147.67
1000.01	1300	500	459.6171	459.6217	0.8800	159.695
1100	1300	500	437.2373	480.961	0.8485	150.88
1200	1300	500	416.1199	499.3438	0.8222	142.98
1300	1300	500	396.312	515.2056	0.8003	135.81
300	1100	500	150	529.1500	0.9956	48.325
400	1100	500	200	512.3480	0.9894	66.842
500.01	1100	500	250.005	489.895	0.9787	88.125
600	1100	500	300	460.977	0.9619	113.955
700	1100	500	350	424.264	0.9367	147.595
800	1100	500	400	377.492	0.8997	195.75
900	1100	500	408.8118	367.9306	0.8503	216.33
1000.01	1100	500	388.9068	388.9107	0.8073	205.5
1100	1100	500	369.97	406.967	0.7721	195.7
1200	1100	500	352.1014	422.5217	0.7434	186.62
1300	1100	500	335.3409	435.9432	0.7197	178.2
300	900	500	150	424.264	0.9919	73.88
400	900	500	200	403.113	0.9801	104.66
500.01	900	500	250.005	374.162	0.9595	143.44
600	900	500	300	335.41	0.9259	197.75
700	900	500	350	282.843	0.8720	286.95
800	900	500	351.391	281.1128	0.7988	315.05
900	900	500	334.4824	301.0341	0.7382	303.58
1000.01	900	500	318.1965	318.1996	0.6900	292.8
1100	900	500	302.7028	332.973	0.6515	282.35
1200	900	500	288.083	345.6996	0.6206	272.13
1300	900	500	274.5853	356.515	0.5955	262.48
300	700	500	150	316.228	0.9823	128.51
400	700	500	200	287.228	0.9557	193.063
500.01	700	500	250.005	244.944	0.9059	296.018
600	700	500	300	180.278	0.8128	524.68
700	700	500	286.7312	200.7118	0.6973	525.01
800	700	500	273.3041	218.6433	0.6091	525.845
900	700	500	260.1529	234.1377	0.5422	525.14
300	500	500	150	200	0.9480	293.615
400	500	500	200	150	0.8576	568.185
500.01	500	500	223.6059	111.8052	0.6489	1081.16
300	300	500	143.6739	43.1022	0.5931	3116.736

Parametric Study
(P/V Height = 100 nm)

λ (nm)	Part. Diam. (nm)	P-V Height (nm)	X (nm)	Z (nm)	Fraction Exp.Area	Shear (s^{-1})
50	250	100	25	122.474	0.9983	153.015
100	250	100	50	114.564	0.9857	330.735
150	250	100	75	100	0.9480	588.77
200	250	100	88.3911	88.3856	0.8648	856.45
250	250	100	78.0137	97.6671	0.7937	746.91
50	200	100	25	96.825	0.9966	242.29
100	200	100	50	86.603	0.9712	554.48
150	200	100	75	66.144	0.8880	1181.6
200	200	100	70.7257	70.6957	0.7559	1223.95
250	200	100	62.4763	78.0815	0.6763	1096.2
50	150	100	25	70.711	0.9919	444.25
100	150	100	50	55.902	0.9259	1197.8
150	150	100	60.005	44.9933	0.7082	2308.9
200	150	100	53.0089	53.0571	0.5514	2223.7
50	100	100	25	43.301	0.9712	1110.2
100	100	100	44.7214	22.3607	0.6489	5599.2
50	50	100	24.2536	6.0634	0.5782	24173.8

Moment Balance Results For Experimental Data Points

Roughness -	λ (nm)	Part. Diam. (nm)	P-V Height (nm)	X (nm)	Z (nm)	Fraction Exp.Area	Shear (1/s)
CA/AF	823.1263	1100	925.7179	411.563	364.85	0.888879	210.336
CA/AF	823.1263	510	925.7179	233.0095	103.5933	0	-
CA/AF	53.87868	120	125.69832	26.939	53.612	0.979485	798.6
Chrom-12	551.0939	1100	950.645	275.547	475.998	0.970983	100.6
Chrom-12	551.0939	510	950.645	244.9191	70.9904	0.413696	2396.6
Chrom-12	57.52406	120	120.81523	28.762	52.657	0.97478	872

$\lambda = \lambda_1$ for particles with diameter of 1100 nm or 510 nm and $\lambda = \lambda_2$ for particles with a diameter of 120 nm